**Please cite the Published Version**

**Additional Information:** This is an open access article published in Bio-Design and Manufacturing, by Springer.

**RESEARCH ARTICLE**

# Electrospun polyvinyl alcohol fibres incorporating an antimicrobial gel for enzymatically controlled reactive oxygen species release

Joel Yupanqui Mieles[1] · Cian Vyas[1,2] · Evangelos Daskalakis[1] · Mohamed Hassan[1] · James Birkett[3] · Abdalla M. Omar[1] · Gavin Humphreys[4] · Carl Diver[5] · Paulo Bartolo[1,2]

## Abstract

Wounds pose a risk to the skin, our body's primary defence against infections. The rise of antibiotic resistance has prompted the development of novel therapies. RO-101® is an antimicrobial gel that delivers therapeutic levels of hydrogen peroxide ($H_2O_2$), a reactive oxygen species, directly to the wound bed. In this study, electrospinning was used to incorporate RO-101® into a polyvinyl alcohol (PVA) sub-micron fibrous mesh that can act as a delivery agent, achieve a sustained release profile, and provide a barrier against infection. Adequate incorporation of this gel into sub-micron fibres was confirmed via nuclear magnetic resonance spectroscopy. Furthermore, scanning electron microscopy exhibited smooth and uniform meshes with diameters in the 200–500 nm range. PVA/RO-101 electrospun meshes generated $H_2O_2$ in concentrations exceeding 1 mM/(g·mL) (1 mM = 1 mmol/L) after 24 h, and the role of sterilisation on $H_2O_2$ release was evaluated. PVA/RO-101 meshes exhibited antimicrobial activity against both Gram-positive *Staphylococcus aureus* (*S. aureus*) and Gram-negative *Pseudomonas aeruginosa* (*P. aeruginosa*) bacteria, achieving viable count reductions of up to 1 log unit CFU/mm² (CFU: colony-forming units). Moreover, these meshes were capable of disrupting biofilm formation, even against multidrug-resistant organisms such as methicillin-resistant *S. aureus* (MRSA). Furthermore, increasing the RO-101® concentration resulted in higher $H_2O_2$ production and an enhanced antimicrobial effect, while fibroblast cell viability and proliferation tests showed a concentration-dependent response with high cytocompatibility at low RO-101® concentrations. This study therefore demonstrates the potential of highly absorbent PVA/RO-101 meshes as potential antimicrobial wound dressings.

✉ Joel Yupanqui Mieles
  joel.yupanquimieles@manchester.ac.uk

✉ Cian Vyas
  cian.vyas@ntu.edu.sg

✉ Paulo Bartolo
  pbartolo@ntu.edu.sg

1   Department of Mechanical, Aerospace and Civil Engineering, University of Manchester, Manchester M13 9PL, UK

2   Singapore Centre for 3D Printing, School of Mechanical and Aerospace Engineering, Nanyang Technological University, Singapore 639798, Singapore

3   Department of Chemistry, University of Manchester, Manchester M13 9PL, UK

4   Division of Pharmacy and Optometry, University of Manchester, Manchester M13 9PL, UK

5   Department of Engineering, Manchester Metropolitan University, Manchester M13 9PL, UK

**Graphic abstract**
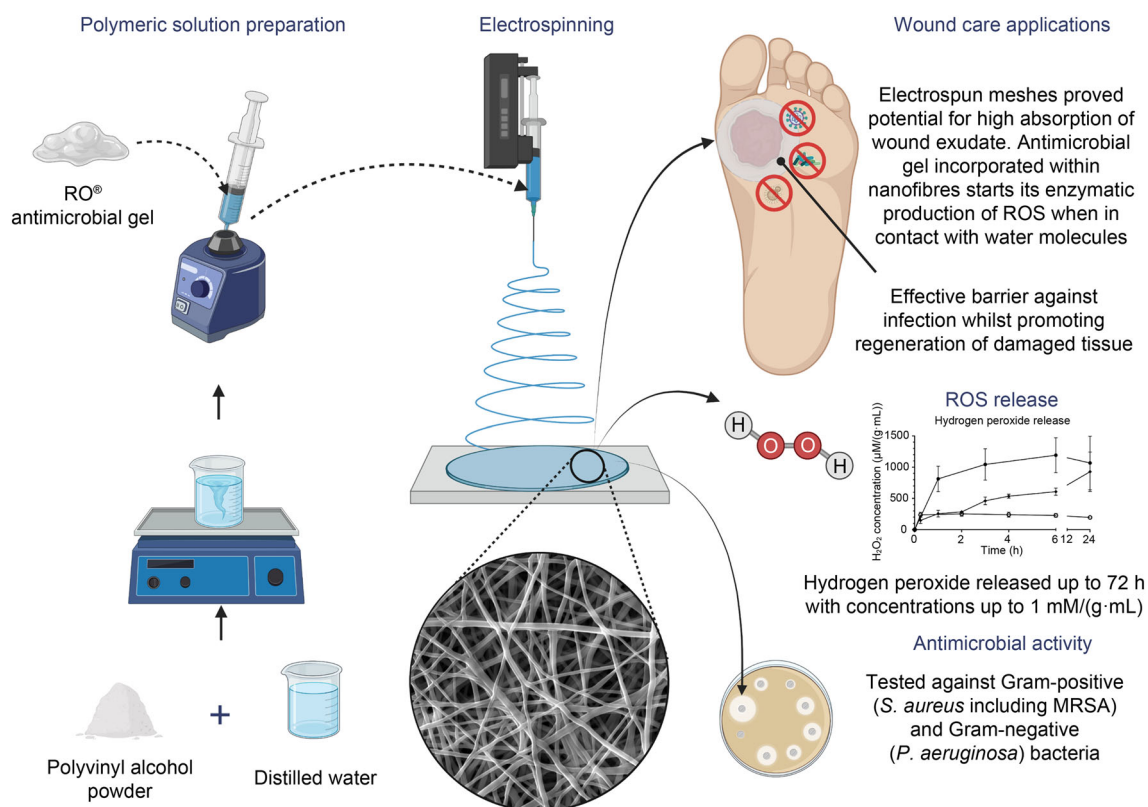


**Keywords** Antimicrobial · Electrospinning · Hydrogen peroxide · Polyvinyl alcohol · Reactive oxygen species · Tissue engineering · Wound dressing

## Introduction

Skin has a natural wound healing capacity through a complex sequence of temporally integrated and overlapping events [1]. However, when this sequence is disturbed (as happens in patients with underlying disease states such as diabetes), the affected area does not heal in a timely and sustainable manner and a chronic wound arises, with the natural healing process interrupted at the inflammation stage. Estimates show that chronic wounds affect 2% of the US population [2], and their treatment costs the US medical system more than $25 billion per year, whilst in the UK, pressure ulcers alone are associated with an annual cost to the National Health Service (NHS) of up to £2.1 billion [3]. Infections of chronic wounds may further delay healing, causing increased pain and reduced patient quality of life, as well as creating an additional financial burden on healthcare systems [2]. Clinically infected wounds can require systemic antibiotic therapy; however, this approach can contribute to the urgent global challenge of antibiotic resistance [2]. Targeted delivery of antimicrobials directly to the wound bed is preferred,

as systemic administration requires doses that can cause serious side effects such as cellular and organ toxicity, allergic reactions, and impacting the composition of the gut microbiome [4, 5]. The incorporation of antimicrobials into wound dressings for local delivery can increase their effectiveness, reduce toxicity, minimise interference with wound healing, and decrease bacterial resistance [4]. The rise of antibiotic resistance also prompts new interest in alternative antimicrobials and wound care products, which is why alternatives such as honey and honey-inspired products have emerged as viable options [6].

Historically, honey has been used in traditional medicine to treat wounds and prevent infection [7]. Several factors make honey an ideal antimicrobial and wound healing biomaterial, including its low water activity, acidity, and phenolic, defensin-1, and methylglyoxal (exclusively present in *Leptospermum*-derived honeys) content [6]. However, the largest contribution to honey's antimicrobial activity comes from glucose oxidase ($GO_x$) and the enzymatic production of reactive oxygen species (ROS) such as hydrogen peroxide

($H_2O_2$). This is due to $GO_x$ catalysing the oxidation of glucose to gluconic acid and $H_2O_2$ (Fig. S1 in Supplementary Information).

Sustained low levels of ROS, such as $H_2O_2$, are essential to wound healing since they provide an antimicrobial barrier between opportunistic pathogens and the wound site, whilst contributing towards important healing mechanisms in each stage of wound healing [8]. During haemostasis, ROS participate in immunocyte recruitment, when their cytotoxic antimicrobial activity is particularly beneficial [9]. During the inflammation stage, ROS are involved in the regulation of matrix metalloproteinases (MMPs) [10, 11], while during the proliferation stage, they support fibroblast proliferation with increased mitogenic rates [12, 13]. Finally, in the remodelling stage, ROS stimulate neutrophils to facilitate highly efficient clearing of damaged tissue, thereby simplifying debridement [14, 15].

Current bioengineering techniques have allowed to replicate honey's $GO_x$ activity and enhance it by controlling the rate of $H_2O_2$ release [16, 17]. For example, Matoke Holdings has patented a ROS (RO®) technology that releases low concentrations of $H_2O_2$ over a sustained duration to effectively kill pathogens without affecting human cells [16, 17]. Moreover, there is no evidence of antibiotic resistance to ROS [16, 17]. This patented technology was developed as a gel formulation, known as RO-101®, which is the antimicrobial agent used for this research. This polymeric gel includes the enzyme $GO_x$ from *Aspergillus niger* and glucose—its substrate—for in situ generation of $H_2O_2$ via enzymatic reaction.

However, the delivery of a gel to a wound bed can cause complications in a clinical environment [6]. As the mode of gel delivery (application and ease of use) and efficacy, including maintaining direct contact with the wound bed, are limited, gels in combination with traditional wound dressings present some constraints such as being absorbed by the dressing, poor penetration into the wound site, and short-term antimicrobial action. Increased volumes of gel would be required to pre-load traditional dressing materials, which may also lead to dressing failure, leakage, and potentially result in further peri-wound skin complications. Most importantly, the delivery of the active agent to the wound site would be minimal and not sustained, requiring frequent dressing changes. Moreover, due to a strong adhesion between traditional dressings and the wound, removal of the dressing is difficult, resulting in additional trauma.

However, biopolymers can be used as a delivery vehicle to support the controlled release of ROS to a wound site, prevent wound dressing leakage and failure, and reduce the possibility of cytotoxicity by achieving a slower, more accurate, and sustained delivery. This has been widely explored with honey through tissue engineering manufacturing processes [6]. For example, ROS-releasing honey-containing scaffolds have been fabricated via electrospinning [18–23], hydrogels and cryogels [24–27], foams [28], powders [29], cement [30], and bioinks [31].

Electrospinning is a simple and well-documented method to produce fibres with sub-micron and nanoscale diameters that can mimic the structure of the natural extracellular matrix [18–23]. This process is a popular approach to fabricate wound dressings and is ideal for ROS release as it allows enzyme immobilisation [32]. $GO_x$ has been encapsulated in polymeric fibres using this method, providing outstanding thermal stabilisation and immobilisation yield [32]. Moreover, electrospun meshes exhibit a high surface-to-volume ratio, which increases the efficiency of the enzyme's catalytic reactions with substrates from the surrounding environment by diffusion [32]. Electrospun meshes also have high porosity with suitable pore size for ultrafiltration, meaning that they form a physical antimicrobial barrier against infection [33], are able to permit adequate permeation of atmospheric oxygen to the wound site, and allow for wound exudate drainage [34]. Furthermore, their high surface-to-volume ratio provides enhanced water absorption, making them exceptional candidates for wound dressings [35]. When hydrophilic polymers are utilised, electrospun sub-micron fibres are capable of absorbing exudate more efficiently than typical film dressings. Electrospinning was therefore selected to incorporate RO-101® gel into the matrix of a biopolymer mesh.

Polycaprolactone (PCL) has been considered to create electrospun fibres for wound dressings due to its biodegradability, mechanical strength, and non-toxicity. However, a harsh solvent is required to create a PCL solution which is not conducive to maintaining $GO_x$ conformation and activity. We have previously demonstrated in a preliminary study that PCL and SurgihoneyRO™ electrospun meshes using acetic acid inhibited the gel's antimicrobial effect and did not support the generation of $H_2O_2$ [36]. Subsequently, biomaterials that require harsh solvents are unlikely to be compatible with $GO_x$ activity, and aqueous solutions are preferred.

An alternative is to use water-soluble polymers as the fibrous matrix to deliver the antimicrobial gel and preserve enzymatic activity. Polymers such as gelatin, alginate, and polyvinyl alcohol (PVA) have been electrospun in combination with honey [18–23]. However, a key limitation is the lack of quantification of ROS generation and the use of natural honey, which is a highly heterogenous and inconsistent material. Thus, there is a requirement for a reproducible and defined ROS generating formulation that can be delivered via a fibrous mesh for wound dressing applications. PVA is hydrophilic, water-soluble, and semi-crystalline with good chemical and thermal stability. PVA is commonly employed for tissue engineering applications since it has tuneable properties (depending on the degree of hydrolysis and molecular weight), facile processing, and good mechanical properties, and it is nontoxic, biocompatible, and biodegradable. Furthermore, it has been designated "generally recognised as

safe" by the US Food and Drug Administration [25, 37]. Subsequently, PVA is often used as a delivery agent for bioactive molecules [38]. This study utilises PVA as the carrier matrix for the antimicrobial RO-101 gel.

The aim of this study is to fabricate a precisely formulated composite electrospun mesh composed of PVA combined with medical-grade RO-101® antimicrobial gel using water as a solvent. The mesh is designed to deliver a controlled and sustained release of $H_2O_2$ for at least 24 h for use in wound dressings and skin tissue engineering applications. Water can dissolve both PVA and RO-101® gel without significantly affecting its enzymatic $H_2O_2$ production, and by replacing commonly used organic solvents, the overall manufacturing process is simpler and less hazardous. This study reports the optimised electrospinning process and characterises the mesh's morphology, chemistry, mechanical and antimicrobial properties, and cytocompatibility. Furthermore, ROS release profiles as a function of RO-101 concentration and sterilisation technique are presented. To the best of our knowledge, this is the first time that a ROS-releasing antimicrobial gel has been successfully encapsulated into biopolymeric sub-micron fibres via electrospinning and validated for $H_2O_2$ production.

## Materials and methods

### Fabrication of electrospun PVA/RO-101 sub-micron fibres

A 0.12 g/mL PVA (molecular weight 89,000–98,000, >99% hydrolysed, Sigma-Aldrich, UK) solution was prepared in deionised water using a hot plate stirrer at 90 °C and 800 r/min overnight. Next, RO-101® antimicrobial gel (Matoke Holdings Ltd., Abingdon, UK) containing 0.01% $GO_x$ was added to the room-temperature PVA solution and vortexed until a homogenous solution was obtained. Importantly, all components were water-soluble (Fig. S2 in Supplementary Information). Triton-X 100 (TX) (Sigma-Aldrich, Gillingham, UK) was then introduced into the polymeric solution (0.5%, mass fraction) to avoid bead formation and improve fibre homogeneity. Throughout this work PVA concentration in water was kept constant at 0.12 g/mL, and RO-101 was incorporated into the PVA solution in gradual increments of mass, as follows: PVA (0 g/mL RO-101 in water), PVA RO20 (0.03 g/mL RO-101 in water), PVA RO30 (0.0514 g/mL RO-101 in water), PVA RO40 (0.08 g/mL RO-101 in water), and PVA RO50 (0.12 g/mL RO-101 in water), making the overall polymeric solutions' concentrations 0.12, 0.15, 0.1714, 0.20, and 0.24 g/mL, respectively. The name of the samples was given based on the theoretical weight concentration that will be present in the electrospun mesh, after the solvent has evaporated. For instance, a 100 mg PVA RO40 mesh contains 40 mg RO-101 (40%, mass fraction) and 60 mg PVA (60%, mass fraction).

A vertical electrospinning system (Spraybase, Maynooth, Ireland) with a blunt-ended 21-gauge needle was used with electrospinning parameters of 17.5 kV, a flow rate of 0.75 mL/h, and a spinneret distance of 13 cm. A rectangular (15 cm × 20 cm) sheet of aluminium foil on top of a stainless-steel plate was used as a collector.

### Viscosity and conductivity measurements

The viscosity of the polymeric solutions ($n = 3$) was measured by a hybrid rheometer (HR-2 Discovery Series, TA Instruments/Waters Corporation, New Castle/Milford, USA) using a parallel plate geometry with a 20 mm diameter and a 0.5 mm gap. Viscosity sweeps were conducted at shear rates from 0.01 to 1000 s$^{-1}$ at 25 °C. The volume of each solution tested was approximately 300 μL.

Conductivity measurements were carried out using a conductivity metre (Jenway Model 4510, Cole-Parmer Instrument Company, UK) at 25 °C. The unit and the cell were calibrated with 0.01 mol/L potassium chloride (KCl) as a standard solution (1413 μS/cm at 25 °C), which provided a cell constant of 0.888 cm$^{-1}$. All tests were performed in triplicate ($n = 3$).

### Sterilisation techniques

Prior to antimicrobial assessment, samples were sterilised using either ultraviolet (UV) or gamma irradiation, and the effect on $GO_x$ activity and mesh morphology was assessed. Samples were standardised to a mass of 100 mg. The electrospun meshes were exposed to UV light for 1 h on each side, in a sterilised cell culture cabinet, or gamma irradiated for a total dose of 25 kGy.

### Scanning electron microscopy (SEM)

The morphology and diameter of the meshes were determined using SEM (Quanta 250, FEI Company, USA) at an accelerating voltage of 10 kV. All samples were stored for 24 h in a vacuum desiccator and then sputter-coated with a 6-nm-thick gold/palladium (80:20) layer (Q150T ES, Quorum Technologies, UK) to produce a conductive surface prior to observation. Images (three per sample, $n = 3$ per group) were collected, and the diameter of at least 50 fibres from each mesh type was assessed quantitatively using NIH ImageJ version 1.53c (Fiji).

## Water absorption capacity, weight loss behaviour, and wettability

A water uptake study was carried out on PVA samples ($n = 3$) with increasing RO-101 gel concentrations (i.e., PVA RO20, PVA RO30, PVA RO40, and PVA RO50) by measuring the degree of swelling. Electrospun samples were cut to $(50 \pm 0.3)$ mg ($m_0$) and submerged in 1 mL of $1\times$ phosphate-buffered saline (PBS) for 1 and 24 h. At the specified time points, soaked samples were placed and flipped gently on filter paper until no excess water was visible. Swollen meshes were measured in triplicate.

To quantify weight loss, the swollen meshes were weighed, and then dried in an oven at 37 °C for 20 h. The swelling and weight loss were calculated according to the following equations:

$$\text{Degree of swelling } = \frac{m_1 - m_0}{m_0} \times 100\%, \tag{1}$$

$$\text{Weight loss } = \frac{m_0 - m_\mathrm{d}}{m_0} \times 100\%, \tag{2}$$

where $m_0$ and $m_1$ are the weights of the meshes before and after soaking in PBS, respectively, and $m_\mathrm{d}$ is the mass of oven-dried meshes.

To evaluate the wettability of PVA/RO-101 electrospun samples, water contact angle measurements of the meshes were taken via the sessile drop method using a drop shape analyser (DSA100, Kruss Scientific, Germany) and deionised water at room temperature. Circular samples ($n = 5$, 19 mm in diameter) were cut from different locations of three electrospun meshes of the same type with one measurement per sample.

## Tensile mechanical testing

The electrospun PVA, PVA RO20, and PVA RO40 meshes tensile mechanical properties were investigated using Instron 3344 and Bluehill software (Instron, Norwood, MA, USA) using a 10 N load cell following ASTM D882-12. Meshes ($n = 6$) were cut into 50 mm × 5 mm (~0.4 mm thick and 100 mg) strips and clamped with an initial grip separation of 25 mm. The meshes were elongated at a rate of 5 mm/min until break. Young's modulus was calculated using the stress–strain curve slope in the initial linear portion (i.e., within 1%–3% strain).

## Nuclear magnetic resonance spectroscopy

To confirm that the method for incorporation of the gel and/or the electrospinning process did not change the chemical structure of RO-101 gel, nuclear magnetic resonance (NMR) spectroscopy was performed on a Bruker Avance 400 NMR spectrometer at 400 MHz ($^1$H) with $D_2O$. $^1$H chemical shifts ($\delta H$) and chemical shifts ($\delta^1 H$) are in parts per million (ppm) relative to internal residual solvent peaks from the stated deuterated solvent.

Pure PVA and RO-101 gel reference samples were collected by $^1$H NMR spectroscopy in $D_2O$. Electrospun mesh materials (i.e., using 50 mg for each individual material per NMR experiment) loaded with RO-101 (i.e., at 20%, 30%, 40%, and 50%) in 1 mL of $D_2O$ were recorded by $^1$H NMR analysis.

## Hydrogen peroxide production

An Amplex® Red assay kit (Fisher Scientific Ltd., Loughborough, UK) was used to determine $H_2O_2$ release in the samples following the manufacturers protocol. Briefly, 154 µg of Amplex Red reagent was dissolved in 60 µL dimethyl sulfoxide (DMSO) and 10 units of horseradish peroxidase (HRP) were dissolved in 1.0 mL of $1\times$ PBS to make stock solutions. The working solution was prepared by mixing 50 µL of Amplex® Red reagent stock solution, 100 µL of 10 U/mL HRP stock solution, and 4.85 mL of $1\times$ PBS to reach a final volume of 5 mL.

In this study, PVA RO20 and PVA RO40 electrospun meshes ($n = 3$) were tested at 0, 1, 2, 3, 6, 24, 48, and 72 h. PVA RO40 (0% $GO_x$) electrospun meshes were used as a negative control. An equivalent mass of RO-101 gel with the same $GO_x$ concentration (0.01%) was used as a positive control. UV and gamma-irradiated samples were compared with nonsterile electrospun meshes to evaluate the effect of the sterilisation method on enzymatic ROS production within the mesh.

Meshes (100 mg) and controls were placed in a 24-well plate and 500 µL of $1\times$ PBS was added. The plate was then kept at room temperature and protected from light. To prevent excess $H_2O_2$ from oxidising the reaction product (resorufin), 10 µL was sampled from each well at each time point and serially diluted (1:5 and 1:25). Standards and diluted samples (50 µL) were loaded into a 96-well plate. The working solution (50 µL) was added to each well containing $H_2O_2$ standards and samples, for a total of 100 µL per well. The reaction mix was incubated inside the plate reader for 30 min at 30 °C shaken for 10 s at 500 r/min every 5 min. The fluorescence was measured for each dilution (at an emission detection of 590 nm/20 nm) using a microplate reader with excitation in the range 530 nm/30 nm (CLARIOstar, BMG Labtech, Germany). The results were normalised for dilution and material mass and presented as µM/(g·mL) (1 µM = 1 µmol/L) $H_2O_2$ (normalised molarity detected as a result of placing 1 g of material in 1 mL of PBS).

## Determination of antimicrobial susceptibility

### Agar diffusion test

Bacterial sensitivity to meshes containing RO-101 was tested using the disc diffusion assay. Mueller Hinton Broth (MHB) and Mueller Hinton Agar (MHA) were purchased from Sigma-Aldrich (Gillingham, UK). Bacterial cultures of *Staphylococcus aureus* (i.e., ATCC 25904, ATCC 6538, and methicillin-resistant *S. aureus*, MRSA) and *Pseudomonas aeruginosa* (i.e., ATCC 15442 and ATCC BAA-47) were prepared overnight and then adjusted to a final optical density (OD) of 0.08. Suspensions were applied uniformly on the surface of an MHA plate to provide a lawn of semi-confluent bacterial growth before placing the sterile electrospun meshes on the plate. Meshes were either 19 mm in diameter (dry) or 100 mg in mass (moistened with 100 μL $1 \times$ PBS). Plates were incubated at 37 °C for 24 h, after which inhibition zones surrounding the mesh were documented.

### 24 h time-kill test

Overnight growth cultures (12 h, 37 °C) of *S. aureus* ATCC 25904 were prepared in MHB and adjusted to a final OD of 0.8 using a spectrophotometer. Sterilised 19-mm-diameter PVA/RO-101 meshes were each placed in a well of 12-well plates (in biological triplicates, $n = 3$). PVA meshes without the RO-101 gel were included as a negative control. Each well containing a mesh was seeded with 2 mL of adjusted bacterial culture. Three empty wells were also seeded as additional controls to monitor normal bacterial growth and compare against wells that contained PVA/RO-101 meshes and determine reduction in bacterial culture. Well plates were incubated at 37 °C under aerobic conditions for 24 h.

Following overnight exposure, the meshes were removed from the broth and placed into sterile universal tubes containing 9 mL sterile MHB with glass beads. Samples were briefly vortexed to detach cells from the mesh surface and serially diluted (1:10) in fresh MHB. Additionally, 1 mL of the remaining bacterial broth culture medium was extracted from each well, serially diluted, and then compared with negative controls (without electrospun meshes). Aliquots (200 μL) were taken from each dilution and inoculated onto agar plates in technical duplicates and incubated overnight (16–18 h) at 37 °C. Images were taken of every plate using a digital single lens reflex (SLR) camera (D3200, Nikon, Japan), and colonies were counted using the "Analyze Particles" function of ImageJ (Fiji, v1.53c). The number of colony-forming units (CFU) was recorded for each dilution where the software was able to accurately count (max 500 colonies in a plate). The data were processed to be expressed as lg(CFU count/mm$^2$), using the area of the meshes available for bacteria to attach (283.53 mm$^2$), and lg(CFU count/mL) for the determination of viable bacteria in bulk medium samples.

### Antibiofilm viability study

Overnight growth cultures (12 h, 37 °C) of MRSA and *S. aureus* ATCC 6538 were prepared in MHB separately, adjusted to a final OD of 0.8, and then diluted 1:100 in sterile MHB. Autoclaved CDC Biofilm Reactor® polycarbonate coupons (BioSurface Technologies, Bozeman, Montana, USA) (12.7 mm in diameter) were placed into a 6-well plate. Bacterial broth culture (4 mL) was then added to each well. Plates were incubated for 48 h at 37 °C to permit biofilm formation on the coupon surface. Coupons were then removed, dip rinsed in sterile PBS (Sigma-Aldrich, Gillingham, UK) and carefully transferred to fresh 6-well plates with each well containing 4 mL sterile MHB. Electrospun meshes ($n = 3$, $(100 \pm 0.3)$ mg each) were added on top of the surface of coupons, ensuring that they were fully submerged in the broth. Coupons and meshes were incubated for 24 h. Upon removal, coupons were dip rinsed in PBS and transferred along with meshes to universal tubes containing 9 mL Dey–Engley neutralisation broth (Sigma-Aldrich, Gillingham, UK). Each tube was vortexed to remove attached surface bacteria. A 1:10 serial dilution was performed on biofilm samples and 200 μL of each dilution was plated onto agar in technical duplicates. Viable count was then calculated and expressed in lg(CFU/mm$^2$) using the area of the coupons (530.93 mm$^2$).

### Cell culturing and cytocompatibility

Human dermal fibroblasts (HDFs) were cultured with Dulbecco's modified Eagle medium (DMEM) (high glucose and GlutaMAX) supplemented with 10% (volume fraction) foetal bovine serum (FBS) and 1% (volume fraction) penicillin/streptomycin and incubated in a cell culture incubator (i.e., 37 °C, 5% CO$_2$, and 95% humidity) until reaching 80% confluence, after which cells were harvested using 0.05% trypsin–EDTA (ethylene diamine tetraacetic acid) at Passage 5. HDFs were then seeded at a density of 10,000 cells per well (in 24-well plates) and were allowed to attach for 24 h. Gamma sterilised PVA, PVA RO20, and PVA RO40 meshes (~19 mm in diameter and 100 mg in mass) were then placed into the culture media on top of the cells and studies were performed on Days 1, 3, and 7 after mesh placement. Cell culture medium was changed every two days.

The metabolic activity of cells ($n = 4$) was evaluated using Alamar Blue resazurin assay (Sigma-Aldrich, Gillingham, UK). At each time point, AB solution (0.1 mg/mL) equal to 10% of the total media by volume was added to each well

and incubated for 4 h. After incubation, 150 µL of each sample was transferred to a 96-well plate and fluorescence was measured (i.e., 540 nm excitation/590 nm emission wavelength) using a plate reader (Infinite 200, Tecan, Männedorf, Switzerland). Samples were then washed in PBS and new medium was added.

The MTT assay (Sigma-Aldrich, Gillingham, UK) was used to assess cell proliferation ($n = 4$) following the manufacturer's instructions. The culture medium was removed, and 150 µL of DMEM (without phenol red) and 150 µL of MTT reagents were added and incubated for 3 h at 37 °C. The solution was removed and 450 µL of MTT solvent was added and shaken in the dark for 15 min at 37 °C. The absorbance was measured (590 nm) using a plate reader.

Cell viability was assessed using a Live/Dead assay kit (ThermoFisher Scientific, UK) according to the manufacturer's instructions. Briefly, medium was removed from the samples and washed with PBS before adding a PBS solution containing 2 µmol/L calcein-AM and 4 µmol/L ethidium homodimer-1. Next, samples were incubated for 30 min and imaged with a confocal fluorescence microscope (Leica TCS SP8, Leica Microsystems, Germany).

The cell nucleus was stained with 4′,6-diamidino-2-phenylindole (DAPI; Thermo Fisher Scientific, Gillingham, UK) to assess cell proliferation. Briefly, the cells were fixed with 10% formalin for 30 min, washed in PBS, permeabilised in 0.1% (volume fraction) TX solution for 5 min, washed in PBS again, and then finally stained with 300 nmol/L DAPI solution for 5 min. Stained cells were then imaged with a confocal fluorescence microscope.

### Statistical analysis

Statistical analyses were performed using one-way analysis of variance and post hoc Tukey's tests as implemented by GraphPad Prism version 9.4.0 (GraphPad Software Inc., San Diego, CA, USA). For all analyses, $p < 0.05$ ($^*p < 0.05$, $^{**}p < 0.01$, $^{***}p < 0.001$, $^{****}p < 0.0001$) was considered to be statistically significant, and all results were reported as mean ± standard deviation (SD).

## Results and discussion

### Nuclear magnetic resonance spectroscopy

RO-101 gel's NMR spectra were explored to identify its characteristic chemical peak (3.65 ppm) and to verify RO-101's presence within PVA-RO electrospun samples. The NMR spectra for PVA RO20, 30, 40, and 50 samples demonstrate that the RO-101 gel had been successfully incorporated within the polymeric fibres (Fig. 1a). There are no major

changes in the peak positions across these electrospun samples. PVA was found to have partial solubility in $D_2O$ at room temperature, while RO-101 was found to be freely soluble in $D_2O$ at room temperature. NMR data support a linear relationship for the encapsulation of RO-101 into the material with increased loading. It can be observed that the peak signal intensity of RO-101 increased with increasing concentration of RO-101 gel in all samples, as summarised in Fig. 1b.

### Rheology and conductivity of electrospinning solutions

The viscoelastic properties of the polymeric solution are among the key factors that affect the electrospinning process and characterise the fabricated product [39]. Uniform and beadless fibre formation requires the polymer solution to be above the entanglement concentration, i.e. a critical number of chain entanglements [40]. This critical value differs across polymeric systems, and when it is not reached, it either results in electrospraying or in the production of beaded fibres; this is due to capillary breakup of the electrospinning jets by surface tension, as described by the Rayleigh instability [39, 41]. For polymeric solutions, viscosity is usually the most influential property that sets the fibre morphology of the electrospun mesh and determines if the solutions can be electrospun [42]. This property can be controlled by adjusting the concentration of the polymer and other components present in the final solution. If the viscosity is too low, electrospinning will likely result in intermittent polymeric filaments as well as droplets of polymer solution [42]. In general, the more viscous the system, the lower the occurrence of defects in the fibres. However, too high a viscosity may cause flow instability due to high cohesiveness of the solution [39].

Figures 2a–2e show the viscosity values corresponding to a range of shear rates (0.01–1000 s$^{-1}$) for each polymeric solution with increasing RO-101 gel concentration. Observable differences were only recorded at viscosities in the 0.01–10 s$^{-1}$ range. This range corresponds to the estimated maximum shear rate that the polymeric solution would experience when flowing through the tubing for electrospinning (2.12 s$^{-1}$ for a 0.75 mL/h flow rate and a tubing internal diameter of 1 mm). PVA RO50 (0.24 g/mL polymeric solution) showed the highest viscosities across the 0.01–10 s$^{-1}$ range (Fig. 2e), with an average of (1.012 ± 0.3) Pa·s at 1.58 s$^{-1}$. The lowest viscosities correspond to PVA (0 g/mL RO-101 gel) with an average of 0.637 Pa·s at the same shear rate (Fig. 2a). Since the PVA concentration remained constant, it was expected that an increase in RO-101 gel would make the solution more viscous. In the range of shear rates that are applicable to the electrospinning process, the polymeric solutions increase in viscosity with increasing RO-101 concentration. It is worth noting that all the solutions were
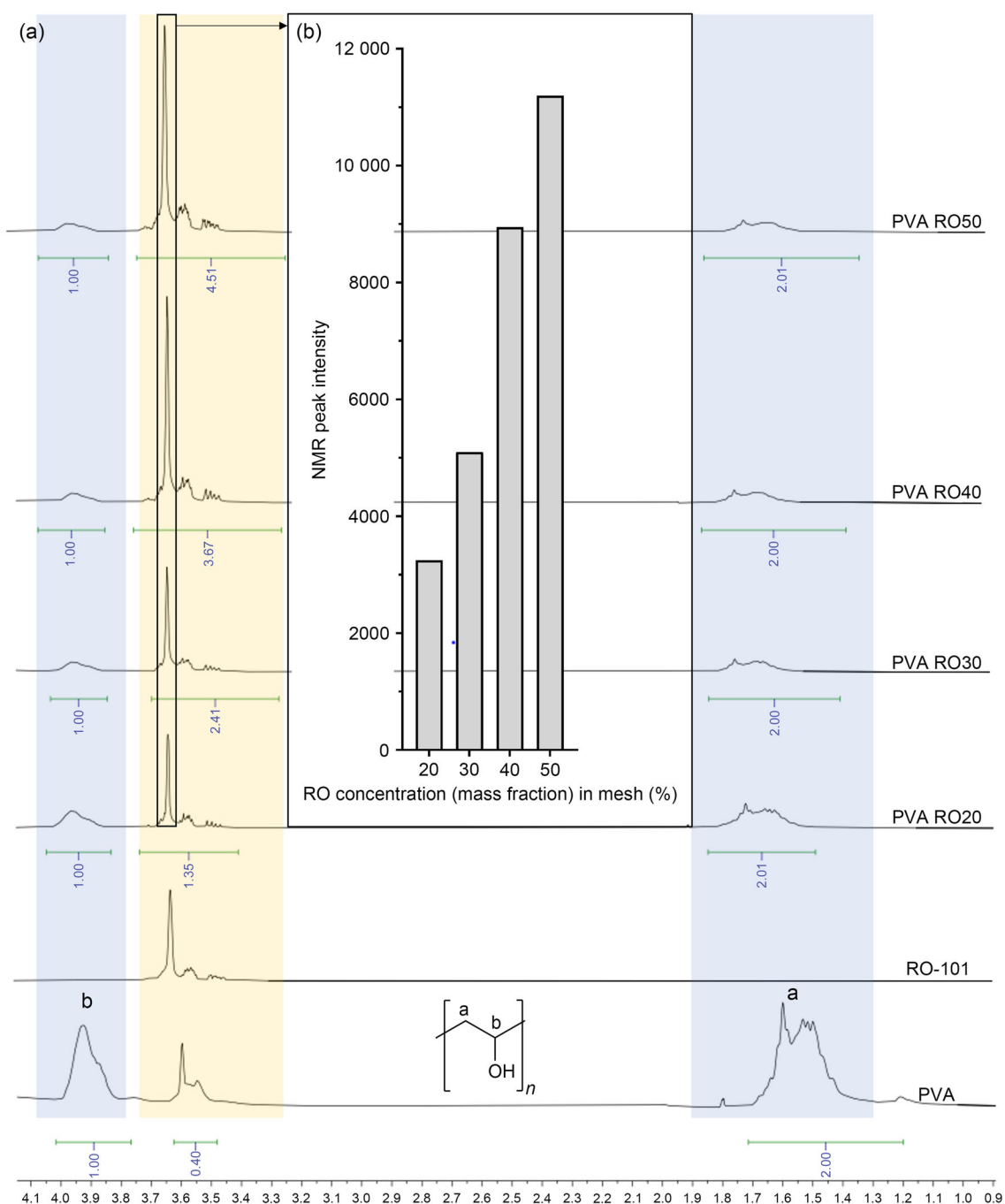
**Fig. 1** **a** $^1$H NMR spectra of PVA RO50, PVA RO40, PVA RO30, PVA RO20, RO-101, and PVA (top to bottom), confirming the encapsulation of the RO-101 gel. **b** NMR peak intensity increases with RO-101 concentration in electrospun meshes. NMR: nuclear magnetic resonance; PVA: polyvinyl alcohol

successfully electrospun, as they fell within the range of viscosities considered suitable for electrospinning (0.1–2.0 Pa·s) [42]. The effect of the increase in viscosity is further illustrated by the differences in the Taylor cones (Fig. 3a), since as the RO-101 gel concentration increases, the Taylor cone becomes less elongated, indicating higher cohesiveness

of the solution. Additionally, no major impact was observed on the viscoelastic flow behaviour of 0.12 g/mL PVA solution when adding 0.5% (mass fraction) TX (Fig. S3 in Supplementary Information).

When measuring the viscosity of different PVA solutions with different concentrations of honey, Tang et al. [18]
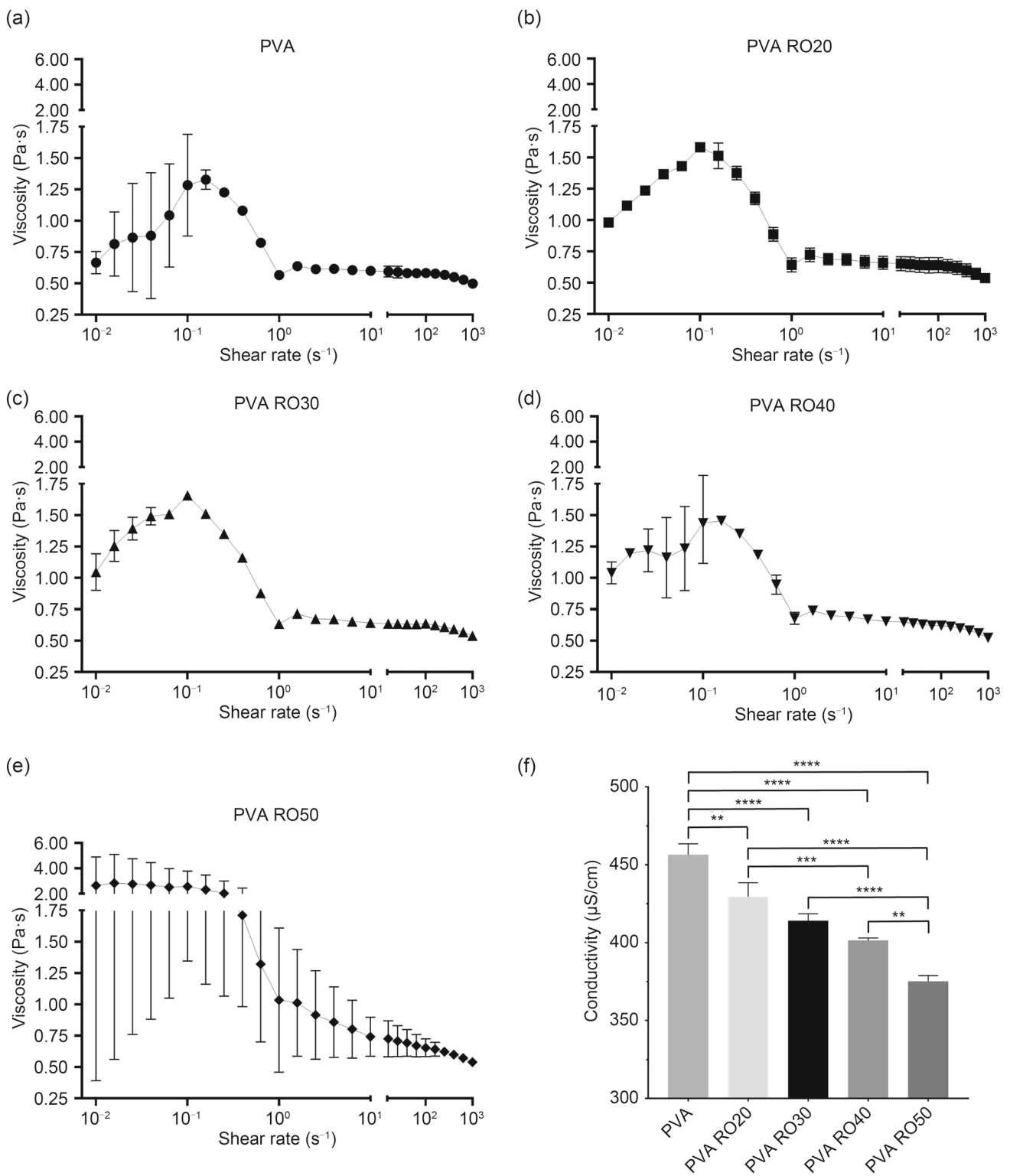
**Fig. 2** **a–e** Rheology and **f** conductivity of PVA solutions with increasing RO-101 concentration. Data are expressed as mean ± standard deviation ($n = 3$; $^{**}p < 0.01$, $^{***}p < 0.001$, $^{****}p < 0.0001$). PVA: polyvinyl alcohol
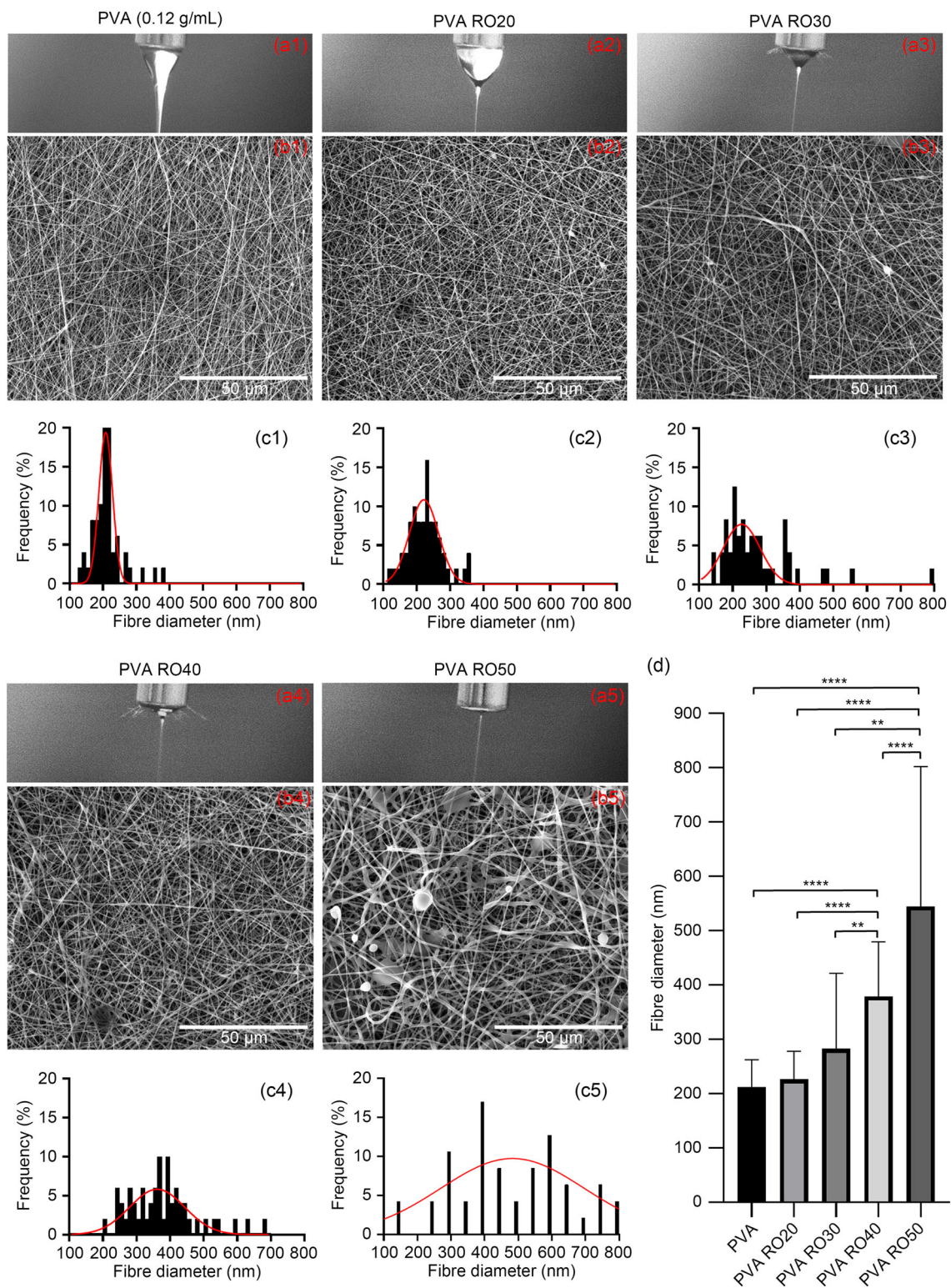
**Fig. 3** **a** Taylor cones, **b** SEM images (magnification: ×2500; scale bar: 50 µm), **c** fibre diameter distribution, and **d** average fibre diameter of electrospun samples with increasing RO-101 gel concentration. Data in (d) are expressed as mean ± standard deviation ($n = 3$; $^{**}p < 0.01$, $^{****}p < 0.0001$). SEM: scanning electron microscopy; PVA: polyvinyl alcohol

reported a decrease in viscosity when increasing the concentration of honey. In their study, the mass of PVA was decreased as the mass of honey was increased. In contrast, our study examined if there was any significant difference in viscosity when increasing the concentration of RO-101 gel in the polymeric solution, whilst maintaining the same mass and concentration of PVA (0.12 g/mL).

Figure 2f shows that as the mass of RO-101 in the polymeric solution is increased (whilst keeping the PVA concentration constant), the conductivity decreases accordingly. The specific conductivity of PVA (0.12 g/mL) was measured at $(456.43 \pm 5.75)$ µS/cm, and the incorporation of larger quantities of RO-101 (ranging from 90–360 mg) reduced the specific conductivities to $(429.50 \pm 7.30)$, $(414.10 \pm 3.65)$, $(401.38 \pm 1.26)$, and $(375.33 \pm 2.93)$ µS/cm for PVA RO20, RO30, RO40, and RO50, respectively. These results are not consistent with previous reports of PVA/chitosan polymeric solutions which incorporated increasing concentrations of honey whilst fixing the PVA concentration within the solution [43]. Contrary to their report, our findings suggest that the number of ions available in the polymeric solution decreases as the mass of RO-101 incorporated increases. From this assay alone, it is expected that there will be an increase in fibre diameter as the mass of RO-101 is increased [44], suggesting that the electrospun sub-micron fibres with the largest diameter will be PVA RO50.

As the concentration of pure PVA increases from 0.08 to 0.10 and 0.12 g/mL, the conductivity of the polymeric solution significantly increases ($p < 0.0001$ for each increment) (Fig. S4 in Supplementary Information). The 0.08, 0.10, and 0.12 g/mL PVA solutions resulted in an average conductivity of $(336.85 \pm 0.98)$, $(403.15 \pm 6.91)$, and $(456.43 \pm 7.03)$ µS/cm, respectively. Moreover, this demonstrated that the addition of the surfactant does not have a significant effect on the conductivity of the polymeric solution ($p = 0.9893$). Incorporating 0.5% (mass fraction) TX into a 0.12 g/mL PVA solution results in an average conductivity of $(452.88 \pm 3.11)$ µS/cm, corresponding to a negligible 0.78% difference.

## Morphologies of electrospun meshes

The fabrication process used for the incorporation of the RO-101 gel into a dressing is environmentally friendly and facile due to the use of water as a solvent to dissolve all components of the electrospinning polymeric solution. The effect of varying PVA, RO-101, and TX (surfactant) concentration on mesh morphology was qualitatively and quantitatively analysed using SEM (Fig. 3).

Pure PVA solutions at 0.12 g/mL were successfully electrospun with a stable jet, a finding that agrees with those of Mwiiri and Daniels [45], who also reported unstable Taylor cones and discontinuous jets during electrospinning for concentrations under 10% and above 12% (mass fraction). To

further verify this, 0.08 and 0.10 g/mL PVA solutions were electrospun, and the morphology of the meshes was analysed (Fig. S5 in Supplementary Information). The average fibre diameters were $(117 \pm 25)$, $(223 \pm 32)$, and $(223 \pm 32)$ nm for the 0.08, 0.10, and 0.12 g/mL solutions, respectively. Thus, fibre diameter increased as the PVA concentration increased from 0.08 to 0.10 g/mL, but there was no significant difference between the 0.10 and 0.12 g/mL solutions (Fig. S5c in Supplementary Information).

The PVA 0.08 g/mL meshes presented an elongated drop configuration, whilst the 0.10 g/mL meshes exhibited decreased elongation and a lower bead occurrence, with beads changing from spherical to spindle-like shape [42]. PVA 0.12 g/mL meshes (Fig. S5a in Supplementary Information) showed an adequate mesh shape and was relatively defect-free when compared to the 0.08 and 0.10 g/mL meshes. This was expected as the viscosity increases with an increase in PVA concentration, and this results in a decrease in defects in the fibres as the polymer concentration reaches its optimal value [39]. The minimum required viscosity, which corresponds to the polymer concentration of the electrospinning solution, depends on the molecular weight of the polymer and the nature of the solvent [42]. The PVA used in this study has a molecular weight of 89,000–98,000, and literature supported the choice of 0.12 g/mL for this specific polymer [45]. Nevertheless, at this concentration, the distribution of fibre diameters was wider (Fig. S5b in Supplementary Information), making it a less uniform and less repeatable mesh. Due to this, as well as other practical challenges (e.g., very high voltages) faced during mesh fabrication, the TX surfactant was added to the polymeric solution to achieve a more stable and consistent electrospinning process.

## Effect of the TX surfactant on stable electrospinning

Electrospinning can only take place when the electrostatic forces from the applied electrical voltage exceed the surface tension of the polymer solution [46]. Low surface tension is advantageous, as a lower voltage is required for the ejection of the jet from the Taylor cone. For PVA aqueous solutions, the surface tension is highly dependent on the degree of hydrolysis of the PVA, with a significant rise in surface tension as the degree of hydrolysis increases [47]. This study employed a fully hydrolysed (>99%) PVA dissolved in water at a high concentration (0.12 g/mL), thus a high voltage (>20 kV) would be required if the composition and all other parameters remain fixed [48]. Working with too high voltages could complicate the fabrication process and lead to a highly unstable jet during electrospinning, as charge density in the solution is too high. To achieve reproducible electrospinning, small amounts of TX surfactant (up to 1% mass

fraction) can be added to lower the surface tension and delay PVA solidification [40, 47, 49].

A comparison between 0%, 0.5%, and 1% (mass fraction) TX was carried out to determine a satisfactory surfactant concentration (Fig. S6 in Supplementary Information). No significant changes were observed in the average fibre diameter of meshes in response to increasing TX concentration (Fig. S6c in Supplementary Information). However, there was a visible improvement in the quality of meshes containing 0.5% (mass fraction) TX compared to that without TX. Specifically, the fibre density increased, the fibre diameter distribution became considerably narrower (Fig. S6b in Supplementary Information), and meshes were electrospun defect-free consistently. Additionally, the voltage required for visually optimal Taylor cone formation was reduced from 22 to 18 kV. This concentration of TX was also suggested by Tiwari and Venkatraman [40] in core–shell electrospinning, where PVA was present within the core. They reported that 0.5% TX reduced interfacial tension and enhanced the transfer of the drag force from the shell to the core solution. This in turn reduced the required threshold ratio between the relative viscosities of the core and shell required for production of uniform sub-micron fibres [40]. Further increase in TX concentration up to 1% (mass fraction) did not have a positive effect on the fabrication process or the mesh morphology. A high occurrence of defects was observed, including a range of bead shapes, from spherical to spindle-like beads, with a relatively low average distance between beads (Fig. S6a in Supplementary Information). This finding is in agreement with the observations by Yao et al. [47] who reported that surface tension decreases significantly in response to a small increase in TX concentration, reaching a critical value at 0.003 g/mL, after which further increase in surfactant concentration had little effect on the surface tension of the polymer solution [47].

PVA electrospun samples (at 0.12 g/mL) including 0.5% (mass fraction) TX result in a uniform, consistently distributed mesh of continuous fibres, free of defects and with repeatable average diameters. This mesh was selected as the baseline for the production of all samples characterised in this study, with further differences mainly reflecting the amount of RO-101 gel added.

## PVA/RO-101 electrospun meshes

Figure 3a shows the differences in Taylor cones when electrospinning PVA (0.12 g/mL) solutions with different concentrations of RO-101; here the same parameters were used (i.e., 13 cm needle-to-collector distance, 0.75 mL/h flow rate, and 17.5 kV applied voltage) for all comparisons. As the RO-101 mass is increased in the polymeric solution, the elongation of the Taylor cone is diminished, reaching a controllable jet in PVA RO30 (0.0514 g/mL RO-101) and PVA

RO40 (0.08 g/mL RO-101) solutions. The decrease in elongation can be explained by the reduction in surface tension and/or drag forces within the polymeric solution. This reduction in tension may be supported by the increasing mass of TX present in the solution as the mass of RO-101 also increased, while the PVA concentration remained constant. This is because small increments in the TX mass may cause considerable reduction in the surface tension of polymeric solutions containing high amounts of RO-101. This claim is supported by an observed decrease in the critical voltage required for jet formation from the Taylor cone [45] that was observed as the mass of RO-101 was increased; this finding is contrary to the expected increase in critical voltage that would be expected as the concentration of the polymeric solution increased [48]. Moreover, the chemical composition of the polymeric RO-101 gel combined with its proportional increase in mass in the solution may contribute to the reduction in drag forces between PVA and the gel, hence reducing the critical voltage for uniform fibre formation [40].

Figures 3b and 3c present the morphology and diameter distributions, respectively, of PVA and PVA/RO-101 electrospun sub-micron fibres with different gel concentrations. It was evident that the average diameter of the sub-micron fibres increased with increasing concentration of RO-101, which was expected as the increase in gel mass leads to an overall increase in the concentration of the polymeric solution; this finding is consistent with those of previous studies [18, 48, 50]. Pure PVA sub-micron fibres (containing 0 g/mL RO-101) averaged (212 ± 50) nm in diameter, and even though the solution containing the smallest amount of RO-101 gel (i.e., PVA RO20, 0.03 g/mL RO-101) did not drastically impact the diameter ((226 ± 51) nm)), further increase in RO-101 concentration resulted in a significant increase in fibre diameter ((283 ± 138), (379 ± 99), and (545 ± 255) nm for PVA RO30, 40, and 50, respectively) (Fig. 3d). It was initially predicted that increasing the mass of RO-101 would cause an increase in both the viscosity and conductivity of the polymeric solution [51], and that this behaviour would be a major influence on the morphology of the meshes. Even though viscosity trends between the solutions studied were not clearly defined, the increase in fibre diameters with an increase in RO-101 mass was closely correlated to the decrease in conductivity (Fig. 2f). This confirms the strong relevance of this parameter to mesh morphology, whilst suggesting that there are other factors which influenced the fibres. The presence of bundles and large spindle-like beads in PVA RO50 fibres (Fig. 3b) show that fibres did not dry sufficiently before reaching the collection plate, confirming that the increase in RO-101 may increase the probability of wet fibres when deposited on the plate [52]. This phenomenon was also noted when removing the electrospun mesh from the collector plate, as a relative increase in moisture was

recorded when removing samples with higher RO-101 concentrations. This may be caused by a gradual reduction in the rate at which water is removed from the jet as RO-101 concentration increases [52]. This hypothesis is supported by Taylor cone images (Fig. 3a), which confirmed that with increasing RO-101, the suspended droplet becomes smaller and is therefore less exposed to air. The wetter the fibres, the less they are strained by the electric field when they are deposited, so they are more likely to undergo a solidification process that is influenced by surface tension and relaxation process dictated by the viscoelastic property of the wet fibres [52]. This process explains the undulating morphology observed as the concentration of the RO-101 gel increased.

With electrospinning solutions of increased polymeric concentration (higher RO-101 mass), the Taylor cone solidified faster and the needle tip was clogged, which was also observed in a similar work by Mwiiri and Daniels [45]. Clogging causes the jet to become inconsistent which also contributes to the creation of defects. Increased RO-101 concentration also resulted in greater inconsistency in the fibre diameter, represented by a larger standard deviation in average diameter (Fig. 3c). Pure PVA (0 g/mL RO-101) has a narrow distribution, with almost two-thirds (66%) of fibres measuring 180–220 nm in diameter. Incorporating RO-101 gel resulted in a wider diameter distribution. Most PVA RO20 fibres (72%) fell within the 180–260 nm range. This range continued to broaden and include larger diameters as the RO-101 concentration increases: 200–350, 250–450, and 300–700 nm for the majority (>78%) of PVA RO30, 40, and 50 samples, respectively. This finding agrees with a similar observation by Khan et al. [50], who also conducted an experiment using honey.

All polymeric solutions containing RO-101 were electrospun into uniform three-dimensional (3D) structures (Fig. 3b) that could mimic the structure of the natural extracellular matrix [18]. Out of these, PVA RO20 showed the most homogeneous morphology (narrowest fibre diameter distribution) with smooth fibres and low bead occurrence. However, for this study PVA RO40 was most appropriate as these fibres carry the highest mass of RO-101 that allow for homogenous fibres with low bead occurrence, which is not the case for PVA RO50 (Figs. 3b and 3c).

### Effect of sterilisation on mesh morphology

The role of sterilisation techniques, gamma irradiation and UV irradiation on fibre morphology were assessed, as this could potentially change the performance of the mesh (Fig. S7 in Supplementary Information). By observing the distribution of the fibres and comparing diameters before and after gamma irradiation, it was determined that sub-micron fibres were not significantly affected by this sterilisation technique

(Figs. S7a–S7c in Supplementary Information). The presence of beaded sub-micron fibres with a spindle shape as well as spherical beads after sterilisation could have been caused by the crosslinking, branching, and grafting effects induced by gamma irradiation on the PVA and RO-101 polymer chains [53, 54]. Gamma irradiation has been shown to simultaneously induce polymerisation of organic compounds, crosslinking of PVA, grafting between PVA and adjacent molecules, and immobilisation of $GO_x$ onto a PVA matrix [54]. These reactions may enhance the performance of the mesh towards our intended wound dressing applications, since they may improve its stability when in contact with the aqueous wound environment, as well as promote a steadier rate of $H_2O_2$ release via improved encapsulation of the $GO_x$ enzyme. Nevertheless, higher doses (closer to 100 kGy) or extended exposure of gamma irradiation could cause degradation of the intermolecular hydrogen bonds in PVA, resulting in chain scissions and an accompanying reduction in mechanical strength [53]. The UV-irradiated samples (Fig. S7a in Supplementary Information) showed no major beads present in the meshes, and their overall morphology appeared similar to the nonsterile samples. However, a significant increase in fibre diameter was observed (Fig. S7c in Supplementary Information), which aligns with previously reported results [55]. It is worth mentioning that a high UV exposure power (~20 W) could increase the water absorption abilities of the fibres via crosslinking [55].

Based on this preliminary morphological assessment, it was concluded that gamma irradiation would be a more suitable sterilisation technique for PVA/RO-101 meshes since it displayed an insignificant effect on fibre diameter and distribution. Additionally, it may improve the stability of the mesh via the crosslinking effect it may have on its polymeric chains. Still, UV irradiation cannot be dismissed from this experiment alone, as it resulted in changes to fibre morphology that could be tolerable if the mesh met all requirements for its intended medical application. For a clear understanding of the suitability of these processes, we performed a separate comparison of the effect on the enzymatic activity of the meshes (Sect. "Comparison of sterilisation methods on $H_2O_2$ production").

### Tensile mechanical properties

Tensile mechanical properties of the meshes were investigated to identify the impact of incorporating RO-101 and to evaluate the suitability of RO-containing meshes for wound dressings and tissue engineering applications. Figure 4a illustrates representative strain–stress curves for the PVA, PVA RO20, and PVA RO40 meshes.

The most flexible meshes were PVA RO40 with Young's modulus of $(152.13 \pm 83.70)$ kPa, which was similar to samples without RO-101 (i.e., $(187.94 \pm 107.36)$ kPa for PVA
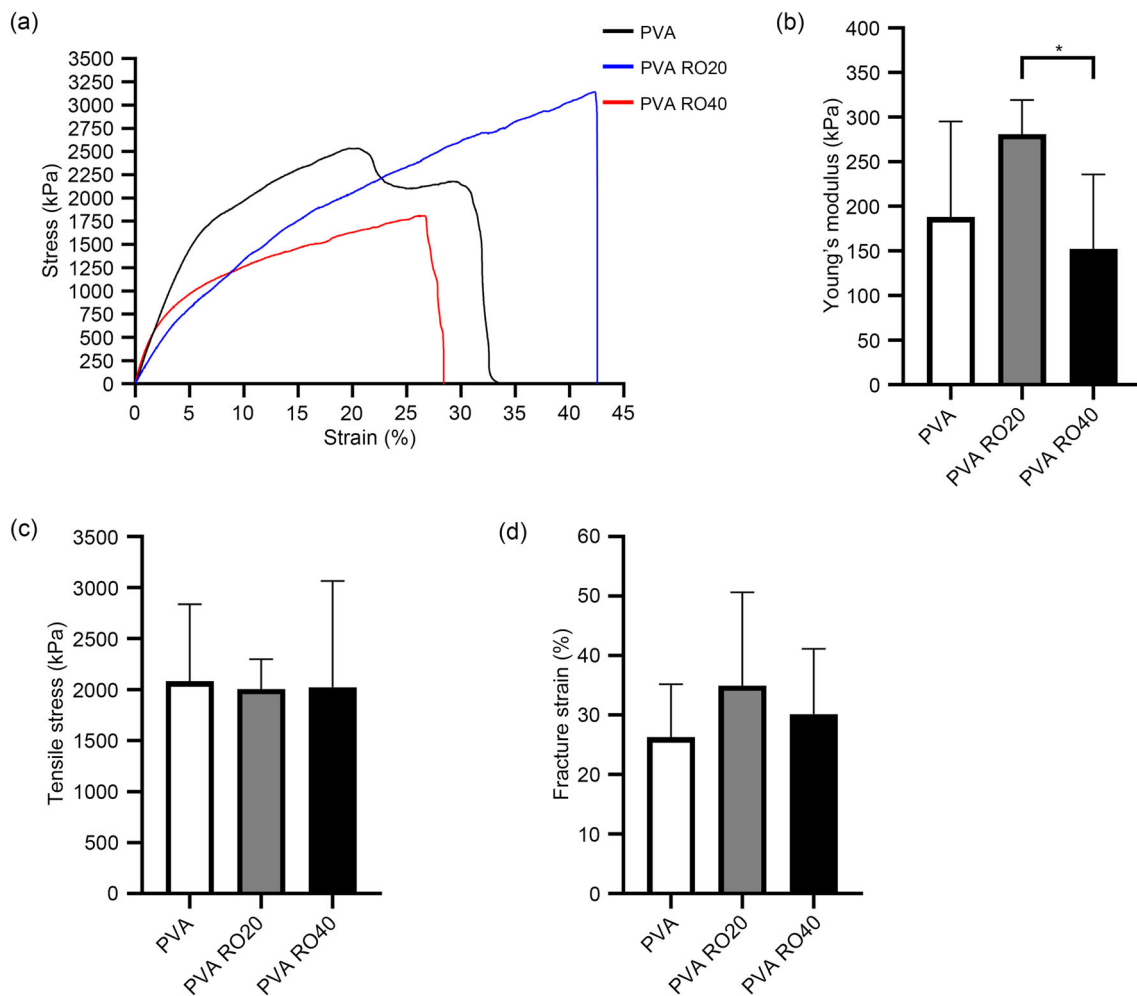
**Fig. 4 a** Representative stress–strain curves of PVA, PVA RO20, and PVA RO40 meshes. Also shown are **b** Young's modulus, **c** ultimate tensile stress, and **d** ductility measurements. Data in (b–d) are expressed as mean $\pm$ standard deviation ($n = 6$; $^{*}p < 0.05$). PVA: polyvinyl alcohol

alone) (Fig. 4b). Conversely, Young's modulus was the highest for the PVA RO20 mesh ((280.83 $\pm$ 38.29) kPa). There was no significant difference in ultimate tensile strength (UTS) values across samples (Fig. 4c). Moreover, PVA RO20 samples demonstrated to be the most ductile with a fracture strain of (34.90 $\pm$ 15.74)% (Fig. 4d). This could be due to PVA RO20 having the most homogeneous morphology (narrowest fibre diameter distribution) as well as smooth fibres and low bead occurrence (Fig. 3). Overall, the ductility decreased with further incorporation of RO-101 into the fibres, with PVA RO40 meshes presenting a mean fracture strain of (30.20 $\pm$ 10.93)%.

Young's modulus of PVA RO40 meshes was found to be similar to that of commercially available wound dressings including Kaltostat®, Aquacel® Ag, Aquacel® Extra, and Exufiber®, which vary between 0.24 and 0.95 MPa [56]. Moreover, the average UTSs recorded for PVA RO20 and PVA RO40 (2.01 and 2.02 MPa, respectively) were significantly higher than the UTSs observed for these commercial

dressings (0.04–0.53 MPa). The electrospinning process presents an approach capable of fine control of the mechanical properties of the meshes and is capable of facilitating improved regeneration by favouring differentiation [57].

## Water absorption capacity, weight loss behaviour, and wettability

The ability to absorb water is an important property for electrospun meshes intended for wound dressing applications, as this represents how much exudate can potentially be absorbed from the wound bed during the healing process [18]. The meshes' ability to absorb wound exudate was estimated by studying their degree of swelling after leaving them to soak for periods of 1 and 24 h in 1× PBS (Fig. 5a). Additionally, as the PVA/RO-101 meshes were uncrosslinked in this study, the stability of the meshes in an aqueous environment was a concern; hence, a weight loss study was performed.
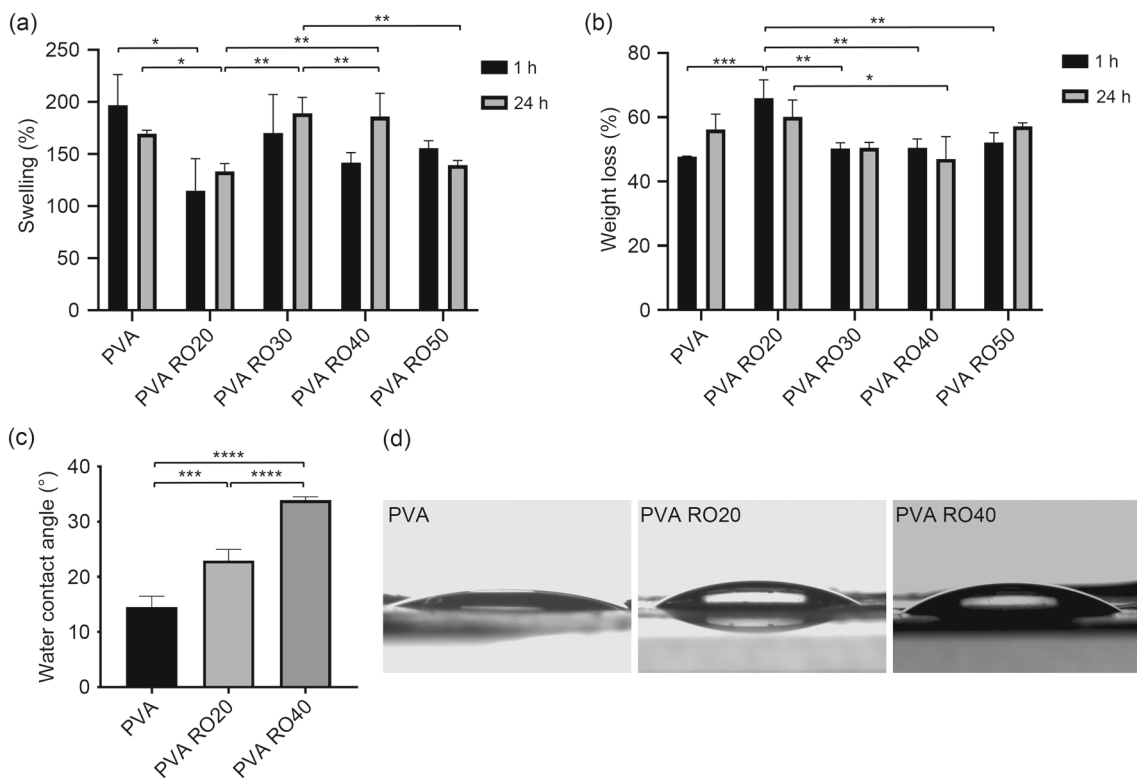
**Fig. 5** Percentages of **a** swelling and **b** weight loss of electrospun PVA meshes with increasing RO-101 concentration following immersion in PBS (pH 7.4) for 1 or 24 h. **c** Water contact angle of PVA meshes with increasing RO-101 concentration and **d** images of droplets on the mesh surface. Data are expressed as mean $\pm$ standard deviation ($n = 3$ for swelling and weight loss and $n = 5$ for wettability; $^{*}p < 0.05$, $^{**}p < 0.01$, $^{***}p < 0.001$, $^{****}p < 0.0001$). PVA: polyvinyl alcohol; PBS: phosphate-buffered saline

After soaking for 1 h, PVA meshes demonstrated the highest average swelling percentage at 197%, followed by PVA RO30 meshes at 170% (Fig. 5a). On the other hand, PVA RO20 samples exhibited the lowest absorption at 115%. After 24 h, PVA RO30 and PVA RO40 showed the largest capacity for absorption with averages of 189% and 186% of their initial mass, respectively. The lowest capacity for absorption was again PVA RO20, which showed an average swelling of 133%.

The deficiency in absorption shown by the PVA RO20 samples can be explained by a large degradation of the fibres when immersed in an aqueous environment. This is supported by the results of the weight loss experiment, where these samples consistently presented the largest average percentage loss in mass, i.e., at 66% and 60% after soaking for 1 h and 24 h, respectively (Fig. 5b). For the 24 h case, the highest swelling percentages found in the PVA RO30 and PVA RO40 samples also relate to the lowest average weight loss percentages, at 50% and 47%, respectively. As expected for the 1 h soaking case, PVA presented the lowest weight loss at 48%. It was evident that PVA has a higher absorption percentage when soaked in PBS for 1 h, as the longer it remains in the aqueous environment, the more quickly it degrades. Conversely, for the PVA RO20, 30, and 40 electrospun meshes, after 1 h the mass of RO-101 gel within the PVA carrying fibres starts to dilute. After 24 h immersion in $1\times$ PBS, at the peak of enzymatic release of $H_2O_2$, the majority of the active ingredient in the RO-101 gel had already reacted, and the concentration of the gel present in the mesh continuously decreased. This created new gaps in the fibres that may then be occupied by molecules of the PVA/RO-101 polymeric chain interacting with water molecules. Moreover, these meshes demonstrated relatively high morphological stability, so with prolonged soaking, composite fibres have the opportunity to swell further without losing as much mass as PVA samples alone. This behaviour led to higher absorption after 24 h of immersion compared to immersion for only 1 h (Fig. 5a). Between 1 and 24 h, an increase in absorption of 16%, 11%, and 31% for the PVA RO20, 30, and 40 electrospun meshes, respectively, was observed. It was also observed that the threshold for RO-101 concentration in the mesh should be 40% (mass fraction), as PVA RO50 electrospun meshes demonstrated a 10% reduction in swelling after 24 h relative to their size after 1 h. This supports the choice of the PVA RO40 mesh as a suitable test case for the intended purposes of this study.

The wettability of electrospun meshes is another important factor that determines their biological performances, as it affects the sample's absorption and $H_2O_2$ release profiles. These parameters are strongly predictive of the capacity of the sub-micron fibres to kill pathogens whilst promoting cell attachment, adhesion, and proliferation. For wound dressings, it is necessary that the surface in contact with the wound bed is hydrophilic (i.e., with a contact angle <90°) [58]. Since PVA RO50 samples were ruled out as a viable option for this study, only PVA RO20 and 40 were analysed. PVA electrospun meshes presented an average water contact angle of $14.50° \pm 1.71°$, whereas the PVA RO20 and PVA RO40 samples exhibited $22.93° \pm 1.76°$ and $33.90° \pm 0.52°$, respectively (Figs. 5c and 5d). A clear trend was observed: as the mass of RO-101 present in the mesh increased, the contact angle was higher, although it remained hydrophilic and retained the potential to act as a wound dressing. These contact angle measurements are aligned with previously reported values, which showed that a mesh of 0.10 g/mL PVA with various molecular weights resulted in contact angles in the 30°–40° range [59, 60], and it is expected that as PVA concentration increases, the contact angle can decrease due to the hydrophilic nature of PVA, which contains hydroxyl groups. Water absorption values of PVA and PVA RO40 were inversely proportional to water contact angles, following the trend suggested by Maver et al. [61]. Overall, PVA presented the lowest contact angle and it resulted in the highest average swelling percentage when compared to PVA RO20 and 40. However, the 3D structure and viscous nature of the materials analysed make the relation between contact angle and water absorption values complicated [61], which may explain why PVA RO20 did not fit the expected trend for the electrospun meshes tested.

After taking these results into consideration, PVA RO40 remained the combination of choice for this study, as it presented an adequate fibre morphology and performed better in wettability and absorption testing than other commercially available materials used for wound dressings such as nonwoven viscose, fibrous alginate, and polyethylene terephthalate [61].

## Enzymatic activity: $H_2O_2$ production

The production of $H_2O_2$ is the dominant factor determining the antimicrobial activity of honey and honey-inspired engineered products [6, 17, 29, 30, 62]. The main objective of this work was to verify that the fabricated meshes would be able to controllably release $H_2O_2$ for at least 24 h, and follow a similar profile as the RO-101 gel would on its own when activated with PBS. Additionally, to enable the translation of the PVA/RO-101 mesh into a clinically viable wound dressing, a suitable sterilisation method is required that does not disrupt

the production of $H_2O_2$. A variety of Food and Drug Administration (FDA)-recognised methods are available, including dry/moist heat, e-beam/gamma/X-ray/UV irradiation, ethylene oxide (ETO) gas perfusion, and $H_2O_2$ vaporisation. Heat is not a suitable method since after only 30 min of incubation at 60 °C, more than 80% of the $GO_x$ activity is lost [63], and the minimum temperature required for moist heat sterilisation is 121 °C or even 176 °C for dry heat sterilisation [64]. Similarly, the basic ETO sterilisation cycle requires an exposure time of 1–6 h at a temperature of 37–63 °C, as well as an 8–12 h mechanical aeration cycle at 50–60 °C to desorb toxic ETO residues present in exposed absorbent materials [65]. Vaporised $H_2O_2$ was not considered as the necessary levels appropriate for sterilisation would oxidise the $GO_x$ thereby rendering it inactive [66]. Therefore, due to the limitations associated with the methods mentioned above, two irradiation sterilisation techniques, gamma irradiation and UV irradiation, were selected. In previous reports, these two methods have been found to not induce substantial changes in the physicochemical and/or cell viability properties of polymeric nanostructures [67].

Subsequently, the effect of either gamma or UV sterilisation on $H_2O_2$ production was assessed in PVA RO20 and PVA RO40 (Fig. 6). These samples were chosen to observe the effect of doubling the concentration of RO present on $H_2O_2$ production.

## Comparison of sterilisation methods on $H_2O_2$ production

Figure 6a provides a comparison of $H_2O_2$ generation over 24 h for UV-sterile, gamma-sterile, and non-sterile PVA/RO-101 samples. After 24 h, non-sterile PVA RO40 samples accumulated a $H_2O_2$ concentration of $(927 \pm 314)$ μM/(g·mL) (referring to $H_2O_2$ molarity produced by 1 g of material when dissolved in 1 mL of PBS), and non-sterile PVA RO20 samples reached $(425 \pm 136)$ μM/(g·mL). As expected, samples with higher RO-101 concentrations reached a significantly higher $H_2O_2$ peak. During the same period, meshes exposed to UV sterilisation reached $H_2O_2$ concentrations of only $(113 \pm 4)$ and $(196 \pm 14)$ μM/(g·mL) for PVA RO20 and 40, respectively. This corresponds to 73% and 79% reductions in $H_2O_2$ levels compared to non-sterile samples, indicating that one hour (on each side) of UV exposure has a strongly adverse effect on mesh $GO_x$ activity. This finding is consistent with previous studies showing that gradual denaturation of $GO_x$ occurs as UV exposure intensity and time increase [68]. Moreover, both UV-sterile samples reached their peak after only 2 h of activation, and this low level was sustained with no further release for the next 22 h. The release profile observed in both UV-sterile samples advises against using this method for sterilisation of PVA-RO electrospun meshes, as they did not meet the key requirement for their intended wound healing application.
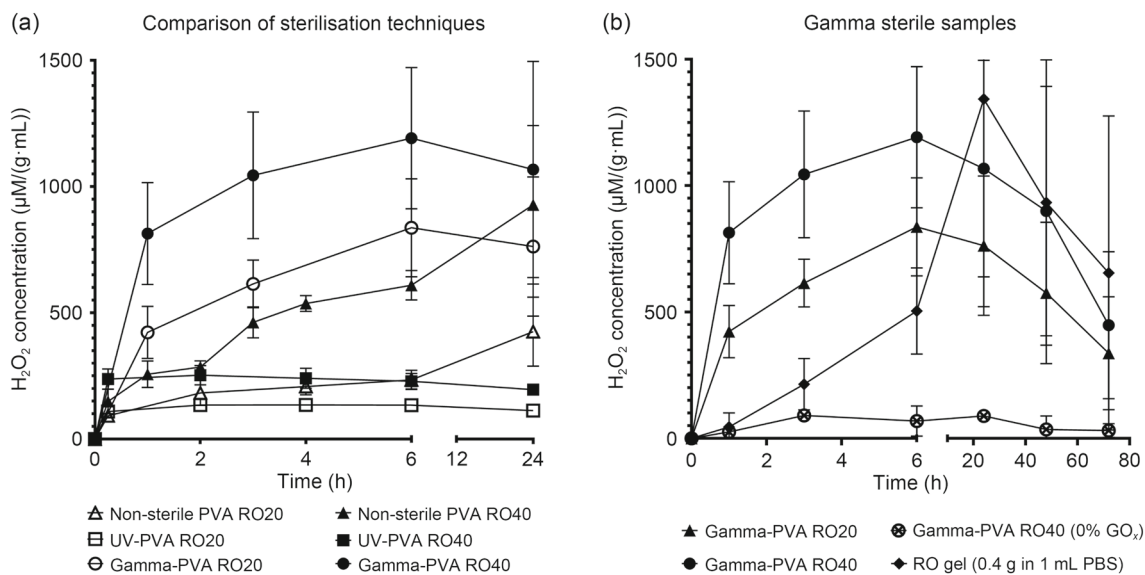
**Fig. 6** $H_2O_2$ production over: **a** 24-h period for non-sterile, UV-sterile, and gamma-sterile electrospun samples (i.e., PVA RO20 and PVA RO40), **b** 72-h period for gamma-sterile PVA RO20 and PVA RO40 electrospun samples, including PVA RO40 (0% $GO_x$) as a negative control and an equivalent mass of RO-101 gel (0.01% $GO_x$) as a positive control. Data are expressed as mean $\pm$ standard deviation ($n = 3$). UV: ultraviolet; PVA: polyvinyl alcohol; $GO_x$: glucose oxidase; PBS: phosphate-buffered saline

Taken together these results demonstrated that gamma irradiation, at a total dose of 25 kGy, had the least effect on $GO_x$ activity, and the overall levels of $H_2O_2$ production achieved were significantly higher than that of UV-sterilised samples. Interestingly, gamma-sterilised samples showed even higher levels of $GO_x$ activity than non-sterile samples during this period. This is in agreement with the hypothesis that there would be little to no detrimental effect of gamma irradiation on $GO_x$ activity [69]. At 24 h, the $H_2O_2$ concentrations of the gamma-sterilised PVA RO20 and 40 electrospun meshes were $(762 \pm 276)$ and $(1067 \pm 428)$ μM/(g·mL), respectively. Even though the $H_2O_2$ concentration at 24 h was slightly higher for gamma-sterile samples, their profiles showed that the peak was reached earlier (between 6 and 24 h). Conversely, non-sterile samples reached their peak at 24 h, which indicates the potential for further $H_2O_2$ release in the following hours. Hence, it was determined that although gamma irradiation did not considerably impact the overall $H_2O_2$ concentration levels, it notably changed the release profile of the samples over the investigated period. It is possible that gamma irradiation immobilised the $GO_x$ onto the mesh, and whilst the entrapment did not have a detrimental effect on enzyme activity [54, 69], it may have promoted a larger initial release followed by a more stable but smaller release over the following 5–10 h, and an earlier drop in $H_2O_2$ production when compared to non-sterile samples.

## 72 h $H_2O_2$ release profiles of gamma-sterilised electrospun meshes

Gamma sterilisation did not exert a major negative impact on the catalytic action of $GO_x$ when evaluated against non-sterile meshes with respect to $H_2O_2$ production over 24 h. Subsequently, a more comprehensive study was carried out over 72 h to verify the levels of $H_2O_2$ that could potentially be achieved by gamma-sterile samples, as well as to help us better understand the $H_2O_2$ release profile. To understand how much $GO_x$ activity was retained after the incorporation of the RO-101 gel into the polymeric solution and during the electrospinning process, an equivalent mass of gamma-sterile RO-101 gel (positive control) was examined at the same time points. A PVA RO40 sample containing 0% $GO_x$ was used as a negative control to identify any potential alternative contributing factor from RO-101.

The PVA RO40 meshes reached a maximum average $H_2O_2$ concentration of $(1192 \pm 280)$ μM/(g·mL) after 6 h of activation. Similarly, the PVA RO20 samples reached their peak at the same time, producing an average of $(837 \pm 194)$ μM/(g·mL), which is approximately 30% lower than PVA RO40 samples (Fig. 6b). This difference was expected because it is assumed that PVA RO20 samples contain approximately 50% less RO-101 mass encapsulated within the fibres. These findings support the claim that gamma irradiation can indeed support RO-101 encapsulation within the fibres, and this improved entrapment may provide a more stable and consistent release profile, as observed by both

meshes. This consistent release profile was achieved without sacrificing the $H_2O_2$ concentration levels expected from the previous evaluation of non-sterilised samples.

Further analysis of release profiles showed that the gamma-sterile electrospun meshes achieved peak production earlier than the RO-101 gel. The gel reached its peak at 24 h, which is similar to the release profile of non-sterilised electrospun samples. In addition, the RO-101 gel was able to maintain higher levels of $H_2O_2$ even after 24 h, with only gradual decreases in concentration from 24 to 48 and 72 h. The gel's ability to sustain high levels of $H_2O_2$ beyond 72 h suggests the potential for the electrospun dressing to extend its intended product application duration for extended periods once the method of incorporating the gel within the fibres is optimised. Furthermore, the release profile of the PVA/RO-101 meshes is influenced by the initial activation and dilution of $GO_x$ during the mixing of the RO-101 gel and the PVA solution before electrospinning. Results suggest that the electrospinning process effectively pauses enzymatic activity by eliminating most of the freely available water. However, $H_2O_2$ levels may be reduced compared to RO-101 gel alone, and there could be resting levels of $H_2O_2$ present within the fibres. Moreover, the influx of oxygen and atmospheric water, to which the electrospun meshes are exposed when not vacuum sealed, may contribute to a further increase in the resting production of $H_2O_2$. Nevertheless, gamma-sterile samples delivered expected $H_2O_2$ levels for up to 24 h, followed by a gradual decline in concentration. This decline is controlled by the decreasing activity of $GO_x$ and the decay rate of $H_2O_2$, and it was slightly steeper in the case of PVA/RO-101 samples than in the gel. In a wound setting, $H_2O_2$ levels would also be reduced by catalase and other peroxidase enzymes, which are abundant in skin tissues [70]. By comparing PVA RO40 meshes to an equivalent mass of RO-101, the addition of 0.1% (mass fraction) TX was confirmed to not have a noticeable negative impact on the enzymatic production of $H_2O_2$, but supported the repeatable and consistent production of meshes. However, its presence in medical devices in the European Union (EU) will become restricted; hence, future work will involve the optimisation of processing to eliminate the need for TX.

The release profiles shown by the gamma-sterile meshes further endorsed gamma irradiation as a potential technique for mesh sterilisation. They also validated the electrospinning process, as the fabricated meshes demonstrated $H_2O_2$ levels comparable to an equivalent mass of RO-101 gel. Although a small percentage of $H_2O_2$ generation occurs during the solution preparation step when mixing the gel, the reaction is paused during the fabrication process via water evaporation. The enzymatic reaction is only resumed once the electrospun mesh is activated with sufficient water molecules. When comparing the average maximum $H_2O_2$ concentration achieved by PVA RO40 samples (i.e., $(1192 \pm 280)$ $\mu M/(g\cdot mL)$) versus the average peak of its equivalent RO-101 gel mass (i.e., $(1343 \pm 821)$ $\mu M/(g\cdot mL)$), there is an estimated loss of 11% (Fig. 6b). Gamma-sterile samples reach peak production faster, which could be a potential advantage for managing a range of wounds. The sharper initial rise and earlier decline do not represent a disadvantage for gamma irradiation, since all samples comply with the minimum requirement of maintaining $H_2O_2$ levels for up to 72 h. This is critical, since it is the maximum time an absorbing wound dressing is generally left in place; however, dressings are typically changed more than once a day depending on the amount of wound exudate [71]. In wounds where a highly concentrated burst of $H_2O_2$ is desired (e.g., infected chronic wounds), gamma-sterile PVA RO40 samples are a highly absorbent solution.

## Antimicrobial susceptibility assays

The efficacy of honey and honey-inspired engineered products has been demonstrated both in vitro and in vivo against a range of Gram-negative and Gram-positive bacteria, including antibiotic-resistant species (e.g., MRSA) [6, 16, 29, 30]. Although further optimisation is required to enhance the incorporation of RO-101 and release profile of $H_2O_2$, antimicrobial assays were carried out to understand the activity of electrospun PVA/RO-101 meshes to inhibit bacterial growth. Agar diffusion tests were performed as an initial qualitative analysis, followed by 24 h time-kill tests, which provided clearer quantitative bactericidal data. Finally, the antibiofilm potency of the electrospun fibres was determined to represent the bacterial growth modes of a chronic wound.

### Agar diffusion test

All electrospun meshes demonstrated potential to inhibit the growth of both staphylococci and pseudomonads. Figures 7a–7c show the zones of inhibition of PVA RO20, 40, and 50 electrospun samples against *S. aureus* (ATCC 25904). The PVA RO20 mesh samples show a zone of inhibition that allowed some colonies to form as well as grow under the mesh. However, as the estimated concentration of RO-101 in the mesh increased from 20% to 40% (mass fraction), the inhibition zone slightly increased. Moreover, in PVA RO40 meshes, approximately half of the mesh degraded into the agar and fully inhibited the growth of the bacteria on these portions (Fig. 7b). The PVA RO50 meshes showed a smaller zone around the mesh, but the portion of the mesh that dissolved was larger, resulting in a larger and clearer zone of inhibition under the mesh itself (Fig. 7c). Although PVA RO50 samples are expected to have a higher antimicrobial effect, they are more challenging to manufacture, and—relative to PVA RO40 samples—result in a thinner mesh when electrospun. Thus, a stronger initial inhibitory effect of PVA

**Fig. 7** Representative images of agar plates showing zones of inhibition by: **a** PVA RO20, **b** PVA RO40, and **c** PVA RO50 in the presence of *S. aureus* (ATCC 25904); **d** 40 mg of RO-101 gel control (at different $GO_x$ concentrations) diluted in 100 µL 1× PBS, **e** PVA RO40, **f** PVA RO40 (100 mg) in the presence of *S. aureus* (ATCC 6538); **g** 40 mg of RO-101 gel control (at different $GO_x$ concentrations) diluted in 100 µL 1× PBS, **h** PVA RO40, **i** PVA RO40 (100 mg) in the presence of MRSA; **j** PVA RO20, **k** PVA RO40 in the presence of *P. aeruginosa* (ATCC 15442); and **l** PVA RO40 in the presence of *P. aeruginosa* (ATCC BAA-47). PVA: polyvinyl alcohol; PBS: phosphate-buffered saline; $GO_x$: glucose oxidase; MRSA: methicillin-resistant *S. aureus*
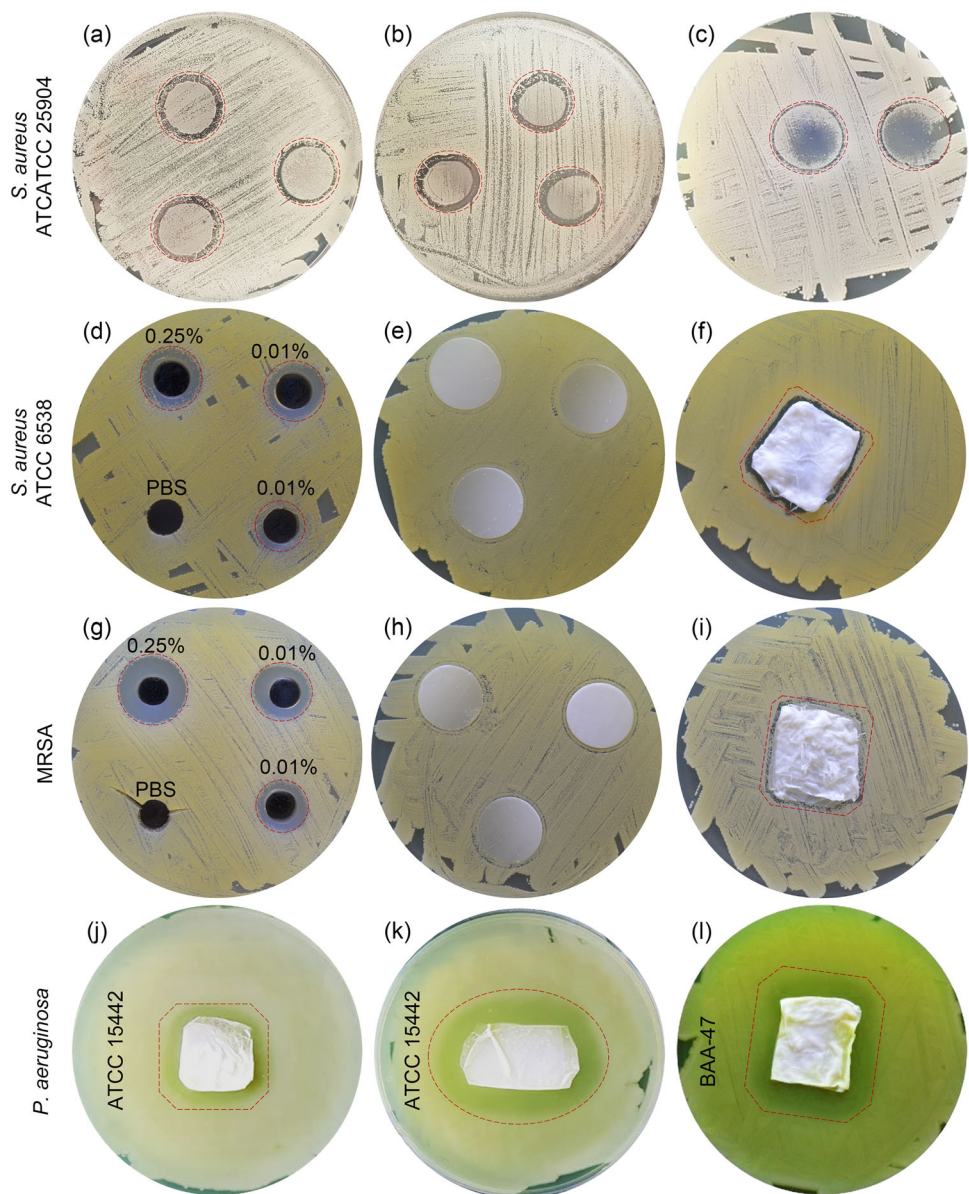


RO50 was observed, but as the fibres began to dissolve in the agar within the 24 h period, bacteria started growing on top and around the mesh.

When evaluating susceptibility against *S. aureus* (ATCC 6538), temporary zones of inhibition were observed around the 19-mm meshes (Fig. 7e), potentially indicating rapid consumption of $H_2O_2$ or minimal activation of the enzymatic reaction due to insufficient free water molecule availability. To verify this, a larger mesh (100 mg) was moistened with 100 µL 1× PBS (Fig. 7f), resulting in a clearer zone of inhibition and suggesting a successful migration of generated $H_2O_2$ into the nutrient agar. The shape and size of the zone could be explained by the tight binding of the antimicrobial gel to the electrospun mesh; accordingly, $H_2O_2$ tended not to diffuse out of the mesh. Moreover, the small zone can be

explained by the fast degradation of $H_2O_2$ once production has stopped, since the moisture available does not support continuous generation. This is further supported by the larger zones of inhibition created by a mass of RO-101 gel that was equivalent to the 100 mg PVA RO40 meshes when both were activated by the same amount of 1× PBS (Fig. 7d). In this case, activated RO-101 gel was added to 8-mm wells in the inoculated agar. This illustrated the antimicrobial activity of the gel at different $GO_x$ concentrations and was used as a positive control to compare to the activity displayed by various meshes regarding the enzymatic generation of $H_2O_2$. PBS was included as a negative control since it was used to activate samples. These zones are much clearer, and fewer colonies were able to grow once the PBS evaporated, indicating a longer period of $H_2O_2$ production. This method

also provided better migration of the antimicrobial gel into the agar, which can be seen by the larger and more circular zone of inhibition. A similar behaviour was observed for the MRSA samples (Figs. 7g–7i). For *P. aeruginosa*, meshes containing RO-101 were unable to fully inhibit growth but presented clear zones in which the concentration of colonies was decreased (Figs. 7j–7l). Finally, the zones became larger as the concentration of RO-101 increased from PVA RO20 to PVA RO40, regardless of the shape of the sample.

Agar diffusion results directly related to previously reported $H_2O_2$ release data and showed that PVA/RO-101 meshes have the potential to inhibit bacterial growth of both Gram-positive and Gram-negative bacteria. This suggests that the proposed mechanism of antimicrobial activity (i.e., $H_2O_2$) is being fulfilled. Next, to generate quantitative data and to conduct an experiment in which the lack of water molecules would not be a problem, a 24 h time-kill test was carried out.

### 24 h time-kill test

Figure 8a shows the antibiotic activity of the 19-mm electrospun meshes when added to a bacterial broth culture medium. Uncrosslinked samples can degrade in aqueous environments, and this may have an impact on the amount of bacteria that can attach to the surface of the mesh. To evaluate the killing effect on bacteria attached to electrospun meshes over 24 h, PVA alone was used as a negative control. PVA samples supported an average lg of CFU count per $mm^2$ of 5.97. In contrast, PVA RO20 samples achieved an average reduction of $(0.77 \pm 0.39)$ log units, whereas PVA RO40 achieved a reduction of $(1.27 \pm 0.31)$ log units. The analysis of viable bacteria remaining in the spent broth culture medium in the wells after removal of the meshes validated the antimicrobial activity of the PVA/RO-101 meshes, as was illustrated by an observable reduction in the CFU count per mL (Fig. 8b). Overall, PVA RO40 achieved an average reduction of $(1.38 \pm 0.39)$ log units when compared to the control (i.e., without an electrospun mesh), and a $(1.00 \pm 0.20)$ log unit reduction when comparing to a well where a PVA sample was added and removed after 24 h, which corresponds to a 90% kill rate.

PVA RO40 meshes not only achieved significant reductions in viable counts compared to PVA alone ($p < 0.01$) but also against PVA RO20 ($p < 0.05$). This set of quantitative data demonstrated a strong relationship between antimicrobial activity and the concentration of RO-101 encapsulated in the mesh. Increasing RO-101 concentration results in an enhancement in antimicrobial activity due to a higher release of enzymatically generated $H_2O_2$ (Fig. 6b). Furthermore, these results aligned with the observations from the agar diffusion test and verified the potential of these meshes as

antimicrobial barriers, particularly for chronic wound management. These wounds are challenging to treat mainly due to the presence of biofilms, which prevent healing and significantly increase the likelihood of infection [72]. Chronic wound biofilms often exhibit resistance towards frequently used antimicrobial agents but are more susceptible to topical antimicrobials after wound debridement [72]. Hence, we subsequently examined the in vitro antibiofilm activity of topically applied PVA/RO-101 meshes against common wound-associated bacteria, including an antibiotic-resistant strain.

### Antibiofilm activity study

In chronic wounds, biofilms impede the transition from inflammation to cell proliferation during healing [72]. PVA/RO-101 meshes can potentially contribute to the healing process since $H_2O_2$ has been successful in resolving biofilm-related infections caused by multidrug-resistant organisms, including MRSA [62]. By delaying biofilm reformation after debridement, PVA/RO-101 meshes may reduce the likelihood of infection and minimise the need for antibiotics and the subsequent risk of antibiotic resistance [72]. Moreover, the generated $H_2O_2$ may simplify debridement in chronic wounds through the activation of neutrophils, which proteolytically remove damaged wound tissue [6].

Figures 8c and 8d show the antibiofilm activity of various electrospun meshes after a 24 h exposure to colonised coupons. For both bacterial strains tested, all samples containing RO-101 (even at concentrations as low as 20% mass fraction) showed a reduction in the CFU count per $mm^2$ of mesh when compared to pure PVA samples. Aligned with previous results, the electrospun samples reported here demonstrated an antibiofilm effect that correlated to their RO-101 concentration and hence their ability to produce $H_2O_2$. Against *S. Aureus* ATCC 6538, PVA RO40 samples achieved the largest reduction in average log CFU count per $mm^2$ at $(0.83 \pm 0.32)$ log units, whilst PVA RO20 samples caused a reduction of $(0.21 \pm 0.40)$ log units (Fig. 8c). Moreover, PVA RO40 achieved significantly greater reductions ($p < 0.0001$) than either PVA or PVA RO20 meshes. Similar statistical differences were observed when testing mesh performance against MRSA. In this case, PVA RO40 samples achieved a reduction of $(0.50 \pm 0.28)$ log units (Fig. 8d), thereby demonstrating signs of antibiofilm activity even against these multidrug-resistant bacteria. PVA RO20 samples were not able to significantly reduce viable counts for either strain, suggesting that there is a minimum effective requirement of RO-101 and $GO_x$ concentration.

To validate our antimicrobial medical device as a suitable therapy against biofilm-related infections, we aimed to achieve a minimal eradication of 99.9% of biofilm-embedded bacteria [73]. This value corresponds to a 3 lg reduction

**Fig. 8** Antibiotic activity of PVA/RO-101 electrospun meshes against *S. asureus* ATCC 25904 after 24 h of incubation: **a** lg CFU count of living bacteria attached to mesh per mm$^2$ and **b** lg CFU count of living bacteria recovered from the culture broth medium following mesh removal, per mL. Antibiofilm activity of PVA/RO-101 electrospun meshes: **c** lg CFU count of remaining viable *S. aureus* ATCC 6538 biofilm on coupons per mm$^2$ and **d** lg CFU count of remaining viable MRSA biofilm on coupons per mm$^2$. Graphs include representative images of CFU count at the same dilution. All graphs show a decrease in viable count as the concentration of RO-101 encapsulated in the mesh increases. Data are expressed as mean ± standard deviation ($n = 3$; $^*p < 0.05$, $^{**}p < 0.01$, $^{***}p < 0.001$, $^{****}p < 0.0001$). PVA: polyvinyl alcohol; CFU: colony-forming units; MRSA: methicillin-resistant *S. aureus*
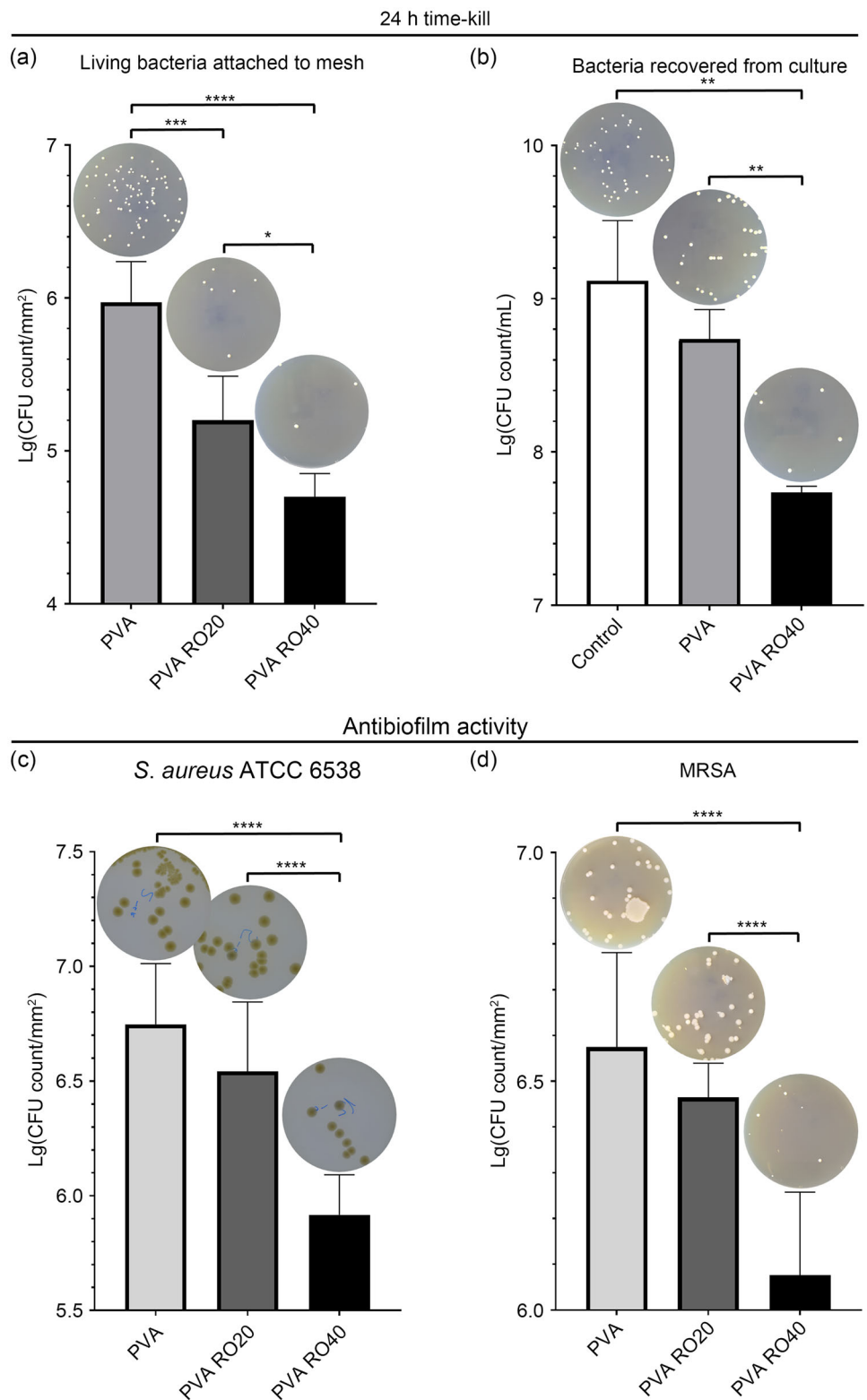


in CFU/mL relative to the control treatment. Although this requirement was not met, our initial results are promising. Greater reductions are expected with larger meshes that contain a higher concentration of RO-101 encapsulated within mesh fibres and after the incorporation process is optimised for a more controlled and sustained H$_2$O$_2$ release. Moreover, testing techniques should continue to be refined and adjusted to the nature of the produced meshes, especially with regard

to difficulties presented by the degradation of the fibres in aqueous environments.

## Cytocompatibility

A preliminary cytocompatibility study was carried out to determine whether there was any potential cytotoxicity induced by the PVA-RO meshes to HDFs. Cell metabolic activity for HDFs exposed to the PVA and PVA RO20 meshes was significantly higher than that of PVA RO40 at all time-points (Fig. 9a), suggesting that exposure to the PVA RO40 mesh induced a decrease in metabolic activity. A similar trend was observed with respect to cell proliferation, which showed a significant decrease in the PVA RO40 group compared to PVA and PVA RO20 from Day 3 onward (Fig. 9b). However, on Day 1, the cell numbers for PVA RO20 and RO40 were similar and were both significantly higher than PVA. These results indicate that exposure to PVA RO40, and specifically to higher levels of $H_2O_2$, contributes to a significant decline in cell activity and number.

This finding was further qualitatively supported by visual observation of a decline in cell nuclei in the PVA RO40 exposure group and a concurrent increase in the PVA and PVA RO20 groups over seven days (Fig. 9c). On Day 1, a similar number of cells were observed; however, by Day 7, only a few cells were visible in the PVA RO40 group, but large numbers of cells were present in the PVA and PVA RO20 groups. Additionally, cell viability tests performed on Day 7 showed that the PVA and PVARO20 groups had large numbers of viable cells that exhibited spindle- and stellate-like morphologies (Fig. 9d). However, the PVA RO40 group showed a considerably lower number of cells and more dead cells were observable. Nevertheless, the presence of live cells suggests that although being exposed to the PVA RO40 mesh induces significant cytotoxicity, the remaining cells can recover once the $H_2O_2$ levels have reduced.

The results indicate that the PVA RO40 meshes induced a cytotoxic response in HDFs cultured for up to seven days that was not observed in either the PVA or PVA RO20 meshes. The levels of $H_2O_2$ peaked within the first 6–24 h and remained at elevated levels for at least 72 h, with the highest levels in PVA RO40 (Fig. 6). Significant cytotoxicity was observed from Day 3 (72 h after exposure to the mesh), which is indicative of cumulative exposure to $H_2O_2$. In contrast, on Day 1 the level of cytotoxicity was unclear. Additional investigation is therefore required to determine the cytotoxicity profile during the initial hours and days after exposure to clearly determine whether cell death occurs via apoptosis or necrosis. Moreover, a cell migration scratch assay is required to provide an in vitro model of wound closure and to examine the role of $H_2O_2$. Furthermore, it should be noted that this study does not replicate a skin wound environment, since the moisture levels in that environment cannot be directly compared to those tested here. In a wound environment, the meshes would not be exposed to such high levels of water, and the activation of the mesh and the generation of $H_2O_2$ would be slower.

Subsequently, an improved in vitro or skin explant model is required to establish the actual $H_2O_2$ release kinetics and to determine specific therapeutic levels. This is key as the concentration of $H_2O_2$ present in the wound tissue affects the rate of healing. For example, in a mouse excision wound model, Loo et al. [74] observed that $H_2O_2$ had a positive effect on angiogenesis and wound closure at a concentration of 10 mmol/L. However, at a higher concentration (i.e., 166 mmol/L), $H_2O_2$ was found to hinder the wound closure process [74]. In another mouse model, the application of 50 mmol/L $H_2O_2$ topically promoted wound closure, whereas the application of 980 mmol/L $H_2O_2$ resulted in delayed healing [75]. Concentrations of $H_2O_2$ below 50 mmol/L thus appear to be more effective in promoting wound healing, and lower concentrations are generally preferred. Here, the PVA RO40 electrospun meshes generated $H_2O_2$ in concentrations over 1 mM/(g·mL) after 24 h; thus, positive wound healing is expected in vivo, although some cytotoxicity was observed in the current in vitro study. Moreover, the optimal concentration of $H_2O_2$ may vary depending on the specific culture environment and cell type involved. Therefore, a range of RO-101 concentrations in the electrospun meshes should be evaluated using in vitro, ex vivo skin explants, and in vivo models to determine the optimal level of $H_2O_2$ production required for wound healing.

## Conclusions

This study demonstrates the successful encapsulation of medical-grade RO-101 antimicrobial gel into PVA electrospun sub-micron fibres to support the controlled and sustained delivery of $H_2O_2$. PVA/RO-101 meshes at different gel concentrations were fabricated via a simple and nontoxic aqueous electrospinning.

First, NMR spectra confirmed that the RO-101 mass mixed in the polymeric solution was incorporated within the fibres, as higher peak intensities were present following increased gel loading. Morphological studies confirmed smooth and uniform meshes that were able to mimic the structure of the natural extracellular matrix, with diameters in the 200–500 nm range. Moreover, increasing the RO-101 concentration resulted in larger average diameter and wider fibre distributions. The selection of PVA as a matrix carrier for RO-101 was further validated by its hydrophilicity and large capacity for absorption, with PVA RO40 samples presenting water contact angles as low as 30° and swelling percentages close to 200% of their initial mass. Taken together, these results support their use in absorbing exudate from the wound bed.
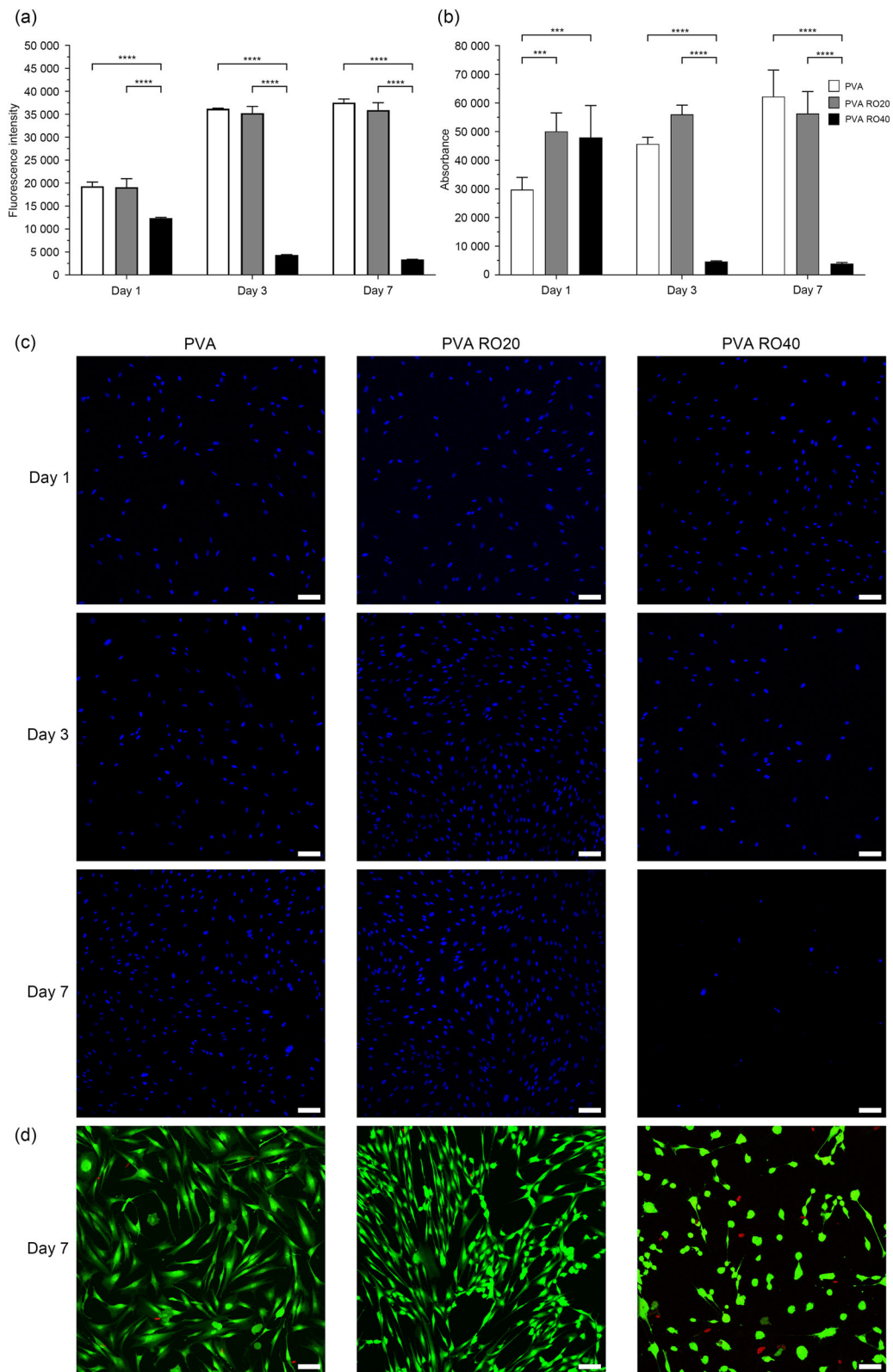
**Fig. 9** Cytocompatibility of HDFs exposed to PVA, PVA RO20, and PVA RO40 meshes, including **a** cell metabolic activity and **b** proliferation on Days 1, 3, and 7. Microscopy imaging of HDFs exposed to PVA, PVA RO20, and PVA RO40 meshes, including **c** cell nuclei staining (blue) on Days 1, 3, and 7, and **d** cell viability (green: live; red: dead) on Day 7 (scale bar: 100 μm). Data are expressed as mean ± standard deviation ($n = 4$; ***$p < 0.001$, ****$p < 0.0001$). PVA: polyvinyl alcohol; HDFs: human dermal fibroblasts

The PVA/RO-101 meshes successfully generated $H_2O_2$ after activation in an aqueous environment. Importantly, higher enzymatic production of $H_2O_2$ was achieved with increasing RO-101 concentration within the mesh. Gamma-sterile PVA RO40 meshes achieved $H_2O_2$ levels comparable to equivalent mass of RO-101 gel, thereby validating the electrospinning process and sterilisation method. Although $H_2O_2$ generation began during the solution preparation phase, the reaction was effectively paused during the electrospinning process via water evaporation. Overall, the PVA RO40 meshes were able to release over 1 mM/(g·mL) $H_2O_2$ after 24 h of activation and maintained at least half of this $H_2O_2$ level over 72 h. The enzymatic production of ROS was converted into antimicrobial activity against both Gram-positive (*S. aureus*) and Gram-negative bacteria (*P. aeruginosa*), including a multidrug-resistant strain (MRSA). These effects were qualitatively shown through zones of inhibition and were measured quantitatively by examining viable count reductions in time-kill and antibiofilm assays. Increasing the concentration of RO-101 in the meshes—and subsequently their ability to produce $H_2O_2$—resulted in enhanced antimicrobial activity. Further optimisation of the synthesis of the PVA/RO-101 solutions and meshes to increase gel loading and improve enzyme activity will enable even higher ROS production and antimicrobial effect.

Additionally, the in vitro cytocompatibility of the PVA/RO-101 meshes showed a concentration-dependent cell response with high viability and proliferation for PVA RO20 but limited cytotoxicity for PVA RO40. Thus, further understanding is required to elucidate the cell response to $H_2O_2$ exposure and its impact on wound healing. Consequently, this knowledge can enable the launching of preliminary in vivo animal studies and will determine the suitability of preclinical studies designed to facilitate clinical translation of this technology.

Overall, this study demonstrates the potential of highly absorbent antimicrobial PVA/RO-101 meshes, which are capable of absorbing wound exudate to generate and sustain enzymatically controlled $H_2O_2$ production over 72 h. The released $H_2O_2$ acts as a powerful antimicrobial barrier, and therefore, these electrospun meshes show promising results for integration into advanced wound dressings.

**Author contributions** JYM: conceptualisation, methodology, investigation, validation, formal analysis, writing–original draft, writing–review and editing, visualisation. CV: conceptualisation, methodology, investigation, validation, writing–review and editing, supervision. ED: investigation. MH: investigation. JB: investigation. AMO: investigation. GH: methodology, validation, writing–review and editing, supervision. CD: conceptualisation, methodology, validation, writing–review and editing, supervision. PB: conceptualisation, methodology, validation, resources, writing–review and editing, supervision, project administration, funding acquisition.

## Declarations

**Conflict of interest** PB is an editorial board member for *Bio-Design and Manufacturing* and was not involved in the editorial review or the decision to publish this article. The authors declare that they have no conflict of interest.

**Ethical approval** This article does not contain any studies with human or animal subjects performed by any of the authors.

## References

1. Han G, Ceilley R (2017) Chronic wound healing: a review of current management and treatments. Adv Ther 34(3):599–610. https://doi.org/10.1007/s12325-017-0478-y
2. Falcone M, De Angelis B, Pea F et al (2021) Challenges in the management of chronic wound infections. J Glob Antimicrob Resist 26:140–147. https://doi.org/10.1016/j.jgar.2021.05.010
3. Dealey C, Posnett J, Walker A (2012) The cost of pressure ulcers in the United Kingdom. J Wound Care 21:261–266. https://doi.org/10.12968/jowc.2012.21.6.261
4. Boateng JS, Matthews KH, Stevens HNE et al (2008) Wound healing dressings and drug delivery systems: a review. J Pharm Sci 97(8):2892–2923. https://doi.org/10.1002/jps.21210
5. Elvers KT, Wilson VJ, Hammond A et al (2020) Antibiotic-induced changes in the human gut microbiota for the most commonly prescribed antibiotics in primary care in the UK: a systematic review. BMJ Open 10(9):e035677. https://doi.org/10.1136/bmjopen-2019-035677
6. Yupanqui Mieles J, Vyas C, Aslan E et al (2022) Honey: an advanced antimicrobial and wound healing biomaterial for tissue engineering applications. Pharmaceutics 14(8):1663. https://doi.org/10.3390/pharmaceutics14081663

7. Majno G (1975) The healing hand: man and wound in the ancient world. Med Hist 20(4):461. https://doi.org/10.1017/S0025727300031604

8. Dunnill C, Patton T, Brennan J et al (2017) Reactive oxygen species (ROS) and wound healing: the functional role of ROS and emerging ROS-modulating technologies for augmentation of the healing process. Int Wound J 14(1):89–96. https://doi.org/10.1111/iwj.12557

9. Dong RN, Guo BL (2021) Smart wound dressings for wound healing. Nano Today 41:101290. https://doi.org/10.1016/j.nantod.2021.101290

10. Caley MP, Martins VLC, O'Toole EA (2015) Metalloproteinases and wound healing. Adv Wound Care 4(4):225–234. https://doi.org/10.1089/wound.2014.0581

11. Majtan J, Kumar P, Majtan T et al (2010) Effect of honey and its major royal jelly protein 1 on cytokine and MMP-9 mRNA transcripts in human keratinocytes. Exp Dermatol 19(8):E73–E79. https://doi.org/10.1111/j.1600-0625.2009.00994.x

12. Al-Jadi AM, Enchang FK, Yusoff KM (2014) The effect of Malaysian honey and its major components on the proliferation of cultured fibroblasts. Turk J Med Sci 44(5):733–740. https://doi.org/10.3906/sag-1303-43

13. Suh YA, Arnold RS, Lassegue B et al (1999) Cell transformation by the superoxide-generating oxidase Mox1. Nature 401(6748):79–82. https://doi.org/10.1038/43459

14. Stricklin GP, Jeffrey JJ, Roswit WT (1983) Human skin fibroblast procollagenase: mechanisms of activation by organomercurials and trypsin. Biochemistry 22(1):61–68. https://doi.org/10.1021/bi00270a009

15. Witkosarsat V, Descampslatscha B (1994) Neutrophil-derived oxidants and proteinases as immunomodulatory mediators in inflammation. Mediat Inflamm 3(4):257–273. https://doi.org/10.1155/S0962935194000360

16. Dryden M, Lockyer G, Saeed K et al (2014) Engineered honey: in vitro antimicrobial activity of a novel topical wound care treatment. J Glob Antimicrob Resist 2(3):168–172. https://doi.org/10.1016/j.jgar.2014.03.006

17. Cooke J, Dryden M, Patton T et al (2015) The antimicrobial activity of prototype modified honeys that generate reactive oxygen species (ROS) hydrogen peroxide. BMC Res Note 8(1):20. https://doi.org/10.1186/s13104-014-0960-4

18. Tang YD, Lan XZ, Liang CF et al (2019) Honey loaded alginate/PVA nanofibrous membrane as potential bioactive wound dressing. Carbohydr Polym 219:113–120. https://doi.org/10.1016/j.carbpol.2019.05.004

19. Sarkar R, Ghosh A, Barui A et al (2018) Repositing honey incorporated electrospun nanofiber membranes to provide anti-oxidant, anti-bacterial and anti-inflammatory microenvironment for wound regeneration. J Mater Sci Mater Med 29(3):31. https://doi.org/10.1007/s10856-018-6038-4

20. Zhang QM, Lin ZS, Zhang WK et al (2021) Fabrication of green poly(vinyl alcohol) nanofibers using natural deep eutectic solvent for fast-dissolving drug delivery. RSC Adv 11(2):1012–1021. https://doi.org/10.1039/d0ra08755f

21. Naeimi A, Payandeh M, Ghara AR et al (2020) In vivo evaluation of the wound healing properties of bio-nanofiber chitosan/polyvinyl alcohol incorporating honey and Nepeta dschuparensis. Carbohydr Polym 240:116315. https://doi.org/10.1016/j.carbpol.2020.116315

22. Parin FN, Terzioğlu P, Sicak Y et al (2021) Pine honey-loaded electrospun poly (vinyl alcohol)/gelatin nanofibers with antioxidant properties. J Text Inst 112(4):628–635. https://doi.org/10.1080/00405000.2020.1773199

23. Kanimozhi S, Kathiresan G, Kathalingam A et al (2020) Organic nanocomposite band-aid for chronic wound healing: a novel honey-based nanofibrous scaffold. Appl Nanosci 10(5):1639–1652. https://doi.org/10.1007/s13204-019-01247-3

24. Tavakoli J, Tang YH (2017) Honey/PVA hybrid wound dressings with controlled release of antibiotics: structural, physico-mechanical and in-vitro biomedical studies. Mater Sci Eng C 77:318–325. https://doi.org/10.1016/j.msec.2017.03.272

25. Shamloo A, Aghababaie Z, Afjoul H et al (2021) Fabrication and evaluation of chitosan/gelatin/PVA hydrogel incorporating honey for wound healing applications: an in vitro, in vivo study. Int J Pharm 592:120068. https://doi.org/10.1016/j.ijpharm.2020.120068

26. Mukhopadhyay A, Rajput M, Barui A et al (2020) Dual cross-linked honey coupled 3D antimicrobial alginate hydrogels for cutaneous wound healing. Mater Sci Eng C 116:111218. https://doi.org/10.1016/j.msec.2020.111218

27. Saberian M, Seyedjafari E, Zargar SJ et al (2021) Fabrication and characterization of alginate/chitosan hydrogel combined with honey and aloe vera for wound dressing applications. J Appl Polym Sci 138(47):51398. https://doi.org/10.1002/app.51398

28. Rajput M, Mandal M, Anura A et al (2020) Honey loaded silk fibroin 3D porous scaffold facilitates homeostatic full-thickness wound healing. Materialia 12:100703. https://doi.org/10.1016/j.mtla.2020.100703

29. Hall TJ, Azoidis I, Barroso IA et al (2021) Formulation of an antimicrobial superabsorbent powder that gels in situ to produce reactive oxygen. Mater Sci Eng C 118:111479. https://doi.org/10.1016/j.msec.2020.111479

30. Hall TJ, Hughes EAB, Sajjad H et al (2021) Formulation of a reactive oxygen producing calcium sulphate cement as an antibacterial hard tissue scaffold. Sci Rep 11(1):4491. https://doi.org/10.1038/s41598-021-84060-9

31. Datta S, Sarkar R, Vyas V et al (2018) Alginate-honey bioinks with improved cell responses for applications as bioprinted tissue engineered constructs. J Mater Res 33(14):2029–2039. https://doi.org/10.1557/jmr.2018.202

32. Leonarta F, Lee CK (2021) Nanofibrous membrane with encapsulated glucose oxidase for self-sustained antimicrobial applications. Membranes 11(12):997. https://doi.org/10.3390/membranes11120997

33. Lev J, Holba M, Došek M et al (2014) A novel electrospun polyurethane nanofibre membrane – production parameters and suitability for wastewater (WW) treatment. Water Sci Technol 69(7):1496–1501. https://doi.org/10.2166/wst.2014.034

34. Maleki H, Gharehaghaji AA, Dijkstra PJ (2013) A novel honey-based nanofibrous scaffold for wound dressing application. J Appl Polym Sci 127(5):4086–4092. https://doi.org/10.1002/app.37601

35. Kang YO, Yoon IS, Lee SY et al (2010) Chitosan-coated poly(vinyl alcohol) nanofibers for wound dressings. J Biomed Mater Res Part B Appl Biomater 92B(2):568–576. https://doi.org/10.1002/jbm.b.31554

36. Aslan E, Vyas C, Mieles JY et al (2022) Preliminary characterization of a polycaprolactone-surgihoneyRO electrospun mesh for skin tissue engineering. Materials 15(1):89. https://doi.org/10.3390/ma15010089

37. Teodorescu M, Bercea M, Morariu S (2019) Biomaterials of PVA and PVP in medical and pharmaceutical applications: perspectives and challenges. Biotechnol Adv 37(1):109–131. https://doi.org/10.1016/j.biotechadv.2018.11.008

38. Rivera-Hernández G, Antunes-Ricardo M, Martínez-Morales P et al (2021) Polyvinyl alcohol based-drug delivery systems for cancer treatment. Int J Pharm 600:120478. https://doi.org/10.1016/j.ijpharm.2021.120478

39. Luzio A, Canesi EV, Bertarelli C et al (2014) Electrospun polymer fibers for electronic applications. Materials 7(2):906–947. https://doi.org/10.3390/ma7020906

40. Tiwari SK, Venkatraman SS (2012) Importance of viscosity parameters in electrospinning: of monolithic and core–shell fibers. Mater

Sci Eng C 32(5):1037–1042. https://doi.org/10.1016/j.msec.2012.02.019

41. Fong H, Chun I, Reneker DH (1999) Beaded nanofibers formed during electrospinning. Polymer 40(16):4585–4592. https://doi.org/10.1016/S0032-3861(99)00068-3

42. Amariei N, Manea LR, Bertea AP et al (2017) The influence of polymer solution on the properties of electrospun 3D nanostructures. IOP Conf Ser Mater Sci Eng 209(1):012092. https://doi.org/10.1088/1757-899X/209/1/012092

43. Sarhan WA, Azzazy HME, El-Sherbiny IM (2016) The effect of increasing honey concentration on the properties of the honey/polyvinyl alcohol/chitosan nanofibers. Mater Sci Eng C 67:276–284. https://doi.org/10.1016/j.msec.2016.05.006

44. Kim SJ, Lee CK, Kim SI (2005) Effect of ionic salts on the processing of poly(2-acrylamido-2-methyl-1-propane sulfonic acid) nanofibers. J Appl Polym Sci 96(4):1388–1393. https://doi.org/10.1002/app.21567

45. Mwiiri FK, Daniels R (2020) Influence of PVA molecular weight and concentration on electrospinnability of birch bark extract-loaded nanofibrous scaffolds intended for enhanced wound healing. Molecule 25(20):4799. https://doi.org/10.3390/molecules25204799

46. Park JC, Ito T, Kim KO et al (2010) Electrospun poly(vinyl alcohol) nanofibers: effects of degree of hydrolysis and enhanced water stability. Polym J 42(3):273–276. https://doi.org/10.1038/pj.2009.340

47. Yao L, Haas TW, Guiseppi-Elie A et al (2003) Electrospinning and stabilization of fully hydrolyzed poly(vinyl alcohol) fibers. Chem Mater 15(9):1860–1864. https://doi.org/10.1021/cm0210795

48. Ding B, Kim HY, Lee SC et al (2002) Preparation and characterization of nanoscaled poly(vinyl alcohol) fibers via electrospinning. Fiber Polym 3(2):73–79. https://doi.org/10.1007/BF02875403

49. Araujo ES, Nascimento MLF, de Oliveira HP (2013) Influence of triton X-100 on PVA fibres production by the electrospinning technique. Fibre Text East Eur 21(4):39–43. https://doi.org/10.1007/s10692-013-9494-0

50. Khan MQ, Lee H, Khatri Z et al (2017) Fabrication and characterization of nanofibers of honey/poly(1,4-cyclohexane dimethylene isosorbide trephthalate) by electrospinning. Mater Sci Eng C 81:247–251. https://doi.org/10.1016/j.msec.2017.08.011

51. Santos C, Silva CJ, Büttel Z et al (2014) Preparation and characterization of polysaccharides/PVA blend nanofibrous membranes by electrospinning method. Carbohydr Polym 99:584–592. https://doi.org/10.1016/j.carbpol.2013.09.008

52. Zong XH, Kim K, Fang DF et al (2002) Structure and process relationship of electrospun bioabsorbable nanofiber membranes. Polymer 43(16):4403–4412. https://doi.org/10.1016/S0032-3861(02)00275-6

53. Jeun JP, Jeon YK, Nho YC et al (2009) Effects of gamma irradiation on the thermal and mechanical properties of chitosan/PVA nanofibrous mats. J Ind Eng Chem 15(3):430–433. https://doi.org/10.1016/j.jiec.2009.02.001

54. Idris S, Bakar AAA, Ratnam CT et al (2017) Influence of gamma irradiation on polymerization of pyrrole and glucose oxidase immobilization onto poly (pyrrole)/poly (vinyl alcohol) matrix. Appl Surf Sci 400:118–128. https://doi.org/10.1016/j.apsusc.2016.12.175

55. Hikmawati D, Maharani NP, Putra AP et al (2020) The effect of ultraviolet exposure on physical properties of electrospun nanofiber membrane based on polyvinyl alcohol and aloe vera. Key Eng Mater 860:244–250. https://doi.org/10.4028/www.scientific.net/KEM.860.244

56. Minsart M, Van Vlierberghe S, Dubruel P et al (2022) Commercial wound dressings for the treatment of exuding wounds: an in-depth physico-chemical comparative study. Burns Trauma 10:tkac024. https://doi.org/10.1093/burnst/tkac024

57. Wang YZ, Armato U, Wu J (2020) Targeting tunable physical properties of materials for chronic wound care. Front Bioeng Biotechnol 8:584. https://doi.org/10.3389/fbioe.2020.00584

58. Eskandarinia A, Kefayat A, Agheb M et al (2020) A novel bilayer wound dressing composed of a dense polyurethane/propolis membrane and a biodegradable polycaprolactone/gelatin nanofibrous scaffold. Sci Rep 10(1):3063. https://doi.org/10.1038/s41598-020-59931-2

59. Ngadiman NHA, Noordin MY, Idris A et al (2015) Influence of polyvinyl alcohol molecular weight on the electrospun nanofiber mechanical properties. Proc Manuf 2:568–572. https://doi.org/10.1016/j.promfg.2015.07.098

60. Salam A, Khan MQ, Hassan T et al (2020) In-vitro assessment of appropriate hydrophilic scaffolds by co-electrospinning of poly(1,4 cyclohexane isosorbide terephthalate)/polyvinyl alcohol. Sci Rep 10(1):19751. https://doi.org/10.1038/s41598-020-76471-x

61. Maver T, Hribernik S, Mohan T et al (2015) Functional wound dressing materials with highly tunable drug release properties. RSC Adv 5(95):77873–77884. https://doi.org/10.1039/c5ra11972c

62. Dryden MS, Cooke J, Salib RJ et al (2017) Reactive oxygen: a novel antimicrobial mechanism for targeting biofilm-associated infection. J Glob Antimicrob Resist 8:186–191. https://doi.org/10.1016/j.jgar.2016.12.006

63. O'Malley JJ, Ulmer RW (1973) Thermal stability of glucose oxidase and its admixtures with synthetic polymers. Biotechnol Bioeng 15(5):917–925. https://doi.org/10.1002/bit.260150509

64. Götz A, Wani AA, Langowski HC et al (2014) Food technologies: aseptic packaging. In: Motarjemi Y, Moy G, Todd ECD (Eds.), Encyclopedia of Food Safety. Waltham, Elsevier, p.124–134. https://doi.org/10.1016/B978-0-12-378612-8.00274-2

65. Association for the Advancement of Medical Instrumentation (1992) Good hospital practice: ethylene oxide sterilization and sterility assurance. ANSI/AAMI ST, 41–1992

66. Greenfield PF, Kittrell JR, Laurence RL (1975) Inactivation of immobilized glucose oxidase by hydrogen peroxide. Anal Biochem 65(1):109–124. https://doi.org/10.1016/0003-2697(75)90497-2

67. Tapia-Guerrero YS, Del Prado-Audelo ML, Borbolla-Jiménez FV et al (2020) Effect of UV and gamma irradiation sterilization processes in the properties of different polymeric nanoparticles for biomedical applications. Materials 13(5):1090. https://doi.org/10.3390/ma13051090

68. House JL, Anderson EM, Ward WK (2007) Immobilization techniques to avoid enzyme loss from oxidase-based biosensors: a one-year study. J Diabetes Sci Technol 1(1):18–27. https://doi.org/10.1177/193229680700100104

69. Gürsel I, Hasirci VN (1992) Matrix entrapment of glucose oxidase by γ irradiation. Biomaterials 13(3):150–155. https://doi.org/10.1016/0142-9612(92)90063-T

70. Kurahashi T, Fujii J (2015) Roles of antioxidative enzymes in wound healing. J Dev Biol 3(2):57–70. https://doi.org/10.3390/jdb3020057

71. Dabiri G, Damstetter E, Phillips T (2016) Choosing a wound dressing based on common wound characteristics. Adv Wound Care 5(1):32–41. https://doi.org/10.1089/wound.2014.0586

72. Alves PJ, Barreto RT, Barrois BM et al (2021) Update on the role of antiseptics in the management of chronic wounds with critical colonisation and/or biofilm. Int Wound J 18(3):342–358. https://doi.org/10.1111/iwj.13537

73. Thieme L, Hartung A, Tramm K et al (2019) MBEC versus MBIC: the lack of differentiation between biofilm reducing and inhibitory effects as a current problem in biofilm methodology. Biol Proced Online 21(1):18. https://doi.org/10.1186/s12575-019-0106-0

74. Loo AEK, Wong YT, Ho RJ et al (2012) Effects of hydrogen peroxide on wound healing in mice in relation to oxidative damage. PLoS ONE 7(11):e49215. https://doi.org/10.1371/journal.pone.0049215

75. Roy S, Khanna S, Nallu K et al (2006) Dermal wound healing is subject to redox control. Mol Ther 13(1):211–220. https://doi.org/10.1016/j.ymthe.2005.07.684